Check for updates

Emerging nanomaterials for the detection of per- and poly-fluorinated substances

Ajith Manayil Parambil, [ID] [a] Eepsita Priyadarshini, [ID] [b] Shounik Paul, [ID] [a] Aristides Bakandritsos, [ID] [ac] Virender K. Sharma [ID] *[d] and Radek Zbořil [ID] *[ac]

Per- and poly-fluoroalkyl substances (PFAS) are manmade chemicals that are extensively used in a wide range of industrial and consumer applications owing to their extraordinary features. However, PFAS are associated with potential risks because of their persistence and bioaccumulation, causing possible harm to human health and ecosystems. In this case, the fabrication of novel sensing technologies is an attractive approach that can address the limitations of conventional chromatographic techniques. Hence, this review highlights the cutting-edge improvements in engineering PFAS nano-sensors, emphasizing the molecular chemistry advancements in optical, electrochemical, aptamer-based, and immune-based nano-sensors. Insights into the tried-and-tested strategies according to the in-depth examination of the detection approach of each nano-sensor at the molecular level are presented. The potential mechanisms of the interactions between PFAS and emerging nanomaterials are presented, including fluorophilic interactions, electrostatic interactions, ion-bridging interactions with divalent cations, hydrophobic interactions, $\pi-\pi$ bonds, hydrogen bonds, ionic exchange, and van der Waals forces in conjunction with materials such as single-atom-supported nanomaterials, carbon dots, graphene, and metallic nanostructures. This review uses an integrated approach to explore the current difficulties and potential in the manufacture of PFAS nano-sensors. Notably, the critical sensor development objectives and the challenges experienced during the process is described. This comprehensive analysis aims to offer a complete viewpoint that may direct future research toward a well-informed and strategic emphasis on enhancing PFAS detection technology. Researchers and practitioners may greatly benefit from these insights, making it easier from them to create innovative and effective PFAS-detecting systems.

1. Introduction

A large class of over 15 000 synthetic compounds known as per- and poly-fluoroalkyl substances (PFAS) is recognized by their strong carbon–fluorine linkages, which endow them with remarkable stability and resistance to degradation.[1–3] PFAS are widely used in consumer goods and operations, making them widespread environmental pollutants.[4,5] They are found in the air, water, soil, and even organisms owing to their extensive usage in nonstick cookware, water-resistant fabrics, firefighting foams, and industrial processes. Other sources are the chemical and textile manufacturing industries. Given that PFAS are resistant to natural degradation processes, they have become prevalent in the ecosystem and pose long-term risks to humans.[6,7] Over 5000 Chemical Abstracts Service (CAS) numbers are categorized as PFAS, and most have unknown identities.[8] Additionally, unknown precursors can break down and contribute to the formation of PFAS.

The increasing presence of PFAS in the environment is a growing concern worldwide.[9,10] PFAS contaminate the environment through direct industrial discharges, runoff from landfills, and wastewater treatment plant effluents, where they persist. Therefore, these substances have been found in almost all environmental matrices, including water sources and aquatic ecosystems, as well as remote regions unaffected by direct industrial activities.[11,12] PFAS contamination has been observed in both urban and rural environments, highlighting the widespread impact of these chemicals.[13,14] Numerous PFAS have the ability to concentrate and accumulate in lower trophic level plants and animals, which are then ingested and bio-accumulated by higher trophic level animals (*i.e.*, top predators), heightening the challenge as their long-term

[a]Nanotechnology Centre, Centre for Energy and Environmental Technologies, VSB-Technical University of Ostrava, 17. Listopadu 2172/15, 708 00 Ostrava-Poruba, Czech Republic. E-mail: radek.zboril@upol.cz

[b]Department of Biotechnology, School of Biosciences and Technology, Galgotias University, Greater Noida, Uttar Pradesh 203201, India

[c]Regional Centre of Advanced Technologies and Materials, Czech Advanced Technology and Research Institute, Palacký University, Olomouc, Šlechtitelů 27, 779 00 Olomouc, Czech Republic

[d]Department of Chemical, Environmental, and Materials Engineering, University of Miami, 1251 Memorial Drive, Miami, Florida 33146, USA. E-mail: vks38@miami.edu

8246 | *J. Mater. Chem. A*, 2025, **13**, 8246–8281

This journal is © The Royal Society of Chemistry 2025

accumulation will continue to raise ecological and health-related concerns over time.[15] In a study in West Virginia, USA, 45 distinct PFAS chemicals in various river otter tissues were taken from several watersheds.[16] The liver had the greatest median content of PFAS, followed by the pancreas, lung, kidney, blood, brain, and muscle. The most common chemicals were perfluoroalkyl sulfonates (PFSAs), which made up 58–75% of the total concentrations, and perfluoroalkyl carboxylates (PFCAs), accounting for 21–35%. Hexafluoropropylene oxide dimer acid (HFPO-DA) was uncommon; however, some PFAS compounds, such as 8 : 2 fluorotelomer sulfonate (8 : 2 FTS) and 10 : 2 FTS, were often detected in the liver and bile. The otters from different watersheds had lower liver amounts of PFAS than those gathered downstream of a fluoropolymer manufacturing site. This study determined that the median whole-body burden of PFAS was 1580 µg with blood levels of PFOS and PFOA above the human toxicity reference values.

Based on probabilistic surveys, 98–99% of the population in the United States has measurable amounts of at least one PFAS in their serum.[17] A data analysis regarding the PFAS concentrations in municipal tap water in Massachusetts revealed a pattern of increasing contamination, with the overall number of fluorinated compounds showing a notable rise of 5 to 320 times over 25 years.[18,19] Moreover, a substantial percentage of up to 94% of these substances are still unknown (also known as undiscovered PFAS). The primary human exposure route, residential drinking water, was first investigated when perfluorooctanoic acid (PFOA) was found in human blood samples (mean concentration of 423 µg L^{-1}) among Americans who were not exposed to these contaminants at work between 2002 and 2005.[20]

PFAS pose a significant concern for both public health and environmental management.[21,22] Thus, efforts to mitigate PFAS contamination require a comprehensive understanding of their environmental occurrence, origins, and modes of transportation, which will inform effective strategies for monitoring, remediation, and regulatory measures.[23,24] It is crucial to consistently monitor and identify PFAS contamination in the air, water, and soil to assess the extent of environmental pollution. Subsequently, policymakers and regulatory agencies can utilize this knowledge to develop effective policies that minimize their impact on ecosystems. Additionally, given the detrimental effects of PFAS on life, identifying sources of exposure is essential for protecting the public well-being.[25] Ongoing monitoring plays a vital role in creating efficient risk management plans, legal requirements, and initiatives focused on public health. Detecting PFAS is a fundamental aspect of informed decision-making aimed at safeguarding both human health and the environment from potential risks associated with these persistent compounds.

A few review articles on PFAS sensors has been previously published, offering a comprehensive summary of the various methods for the detection of PFAS.[26,27] In contrast to these outstanding studies, herein we report the latest developments in PFAS nano-sensor engineering from a molecular chemistry standpoint. Nanoparticles play a pivotal role in sensing, demonstrating significant progress in applications such as

detecting and comprehending the molecular structure of pollutants and addressing challenges in water treatment and pollution prevention.[28,29]

Sensor technologies for detecting PFAS have significantly progressed, with improvements in sensitivity, efficiency, and precision in environmental monitoring being evident. More intricate sensor platforms such as novel molecular detection mechanisms that are nano-enabled and nanoparticle-based sensors have replaced traditional detection methods.[27] These advancements provide improved detection limits up to nano-molar concentrations and real-time monitoring capabilities to expand the array of existing tools for PFAS sensing. However, despite this progression, ongoing development is still necessary for PFAS detection sensor systems due to the challenges posed by the diverse nature of PFAS chemicals and their complex matrices.[30] Continued investigation and invention are required to overcome these limitations and promote the growth of sensors with improved accuracy, specificity, and versatility. This effort is critical in meeting the growing demand for reliable PFAS detection techniques and assuring their usefulness in protecting the environment. Improving sensor technology can strengthen environmental protection efforts and get closer to long-term solutions for efficiently addressing PFAS pollution.

Initially, we provide a concise overview of the physicochemical characteristics of PFAS alongside their classification. We provide a succinct summary of the presently available nanomaterial-based approaches for the detection of PFAS together with their drawbacks that arise in the course of developing new sensors, the objectives that must be remembered, and lastly the nano-sensors that have been created thus far. To present information for readers on how each sensor senses PFAS at the molecular level and to outline the previously tried and tested approaches, we present an in-depth discussion of the detection method for each sensor. After evaluating the literature, our discussion focuses on the potential mechanisms of PFAS interaction comprising fluorophilic interactions, electrostatic interactions, ion-bridging interactions with divalent cations, hydrophobic interactions, π–π bonds, hydrogen bonds, ionic exchange, and van der Waal forces with emerging nano-materials including carbon dots, graphene and metallic nano-structures. Also, we systematically examine the current challenges and opportunities associated with the fabrication of PFAS nano-sensors, adopting an integrative approach. This comprehensive analysis will provide a holistic perspective, guiding future research endeavors toward a more informed and strategic focus.

2. Physicochemical properties of PFAS

PFAS are fluorinated substances containing at least one fully fluorinated methyl (–CF$_3$), a methylene carbon atom (–CF$_2$–), and fully fluorinated alkanediyl (–C$_n$H$_{2n}$–) moieties or aromatic rings. A few exceptions reported thus far include the H/Cl/Br/I atom attached to any carbon atom.[31] With over 4700 PFAS varieties documented in the literature, the predominant

This journal is © The Royal Society of Chemistry 2025

J. Mater. Chem. A, 2025, 13, 8246–8281 | 8247

characteristic among these compounds is an alkyl chain with fluorine as a substituent (C–F bond).[32,33] This creates a plethora of divergent physical properties such as high thermal stability, enhanced chemical stability, strong acidity, and hydrophobic and lipophobic surfactant properties. It is presumed that this difference in the properties of PFAS from their hydrocarbon analogues is due to the incorporation of fluorine groups, and thus to understand their properties first, we need to understand the properties of fluorine and the C–F bond, in particular.

Fluorine appears at $\chi = 4$ on the Pauling electronegativity scale, which is the most electronegative element. Its atomic size is the smallest among the period 2 elements, having an electronic configuration of $1s^2$, $2s^2$, $2p^5$, where it experiences the high nuclear charge of nine protons. Thus, ionization by the removal of an electron to become F^+ is extremely endothermic (-401.2 kcal mol^{-1}) with the 2p electrons held close to the nucleus. Alternatively, fluorine atoms readily accept electrons to attain a noble gas-like configuration with the most exothermic value ($+78.3$ kcal mol^{-1}) among the period 2 elements.[34] Owing to the high electronegativity of fluorine compared to that of carbon, the C–F bond is the strongest bond reported in organic chemistry (105 kcal mol^{-1}), but in PFAS, bond dissociation energy (BDE) calculations revealed that a higher BDE is required to dissociate the C–F in their –CF$_3$ moieties (117.8–123.4 kJ mol^{-1}) than the C–F bonds in their –CF$_2$– moieties (106.4–113.6 kJ mol^{-1}) (Fig. 1A).[35,36] The C–F bond is highly polarised due to the small size of fluorine, thus generating a partial charge over the $C^{\delta+}$ and $F^{\delta-}$ atoms. The resultant electrostatic attraction makes the bond less covalent and more electrostatic (Fig. 1B). Particularly, the electrostatic interaction between the polarized $C^{\delta+}$ and $F^{\delta-}$ atoms further strengthens the bonds, classifying them as persistent organic pollutants (POPs).[37] This argument rationalizes the progressive shortening of the bond observed for fluoromethane upon substitution by fluoro groups and is the shortest for tetrafluoromethane. The polarization of the C–F bonds leads to a change in the H–C–H bond angle in the hydrocarbon. This rationale is based on the valence shell electron pair repulsion (VSEPR) theory, which states that the fluorine group shows an electron-withdrawing effect and pulls the valence electron towards itself, narrowing the F–C–H or F–C–F bonds.

The electron–electron repulsion of the electron-rich C–H bonds of PFAS increases, leading to their widening. On the contrary, the F groups are larger than the H groups, thus introducing steric interaction to widen the F–C–F bond angle, while narrowing the H–C–H bond angle, but this is not the case. Thus, the H–C–H bond angle of methane is 109.5°, which increases to 110.2°, and even widens for difluoromethane to 113.8°.[38] A similar case is fluorosubstituted hydrocarbons, where despite the −ve charge density over the F atoms, the C–F bonds close, and the bond angles decrease with an enhancement in the repulsion between the electron-rich C–C bonds, increasing the bond angle.[39] Besides this comparison of a series of progressive fluorinated methane, difluoromethane has
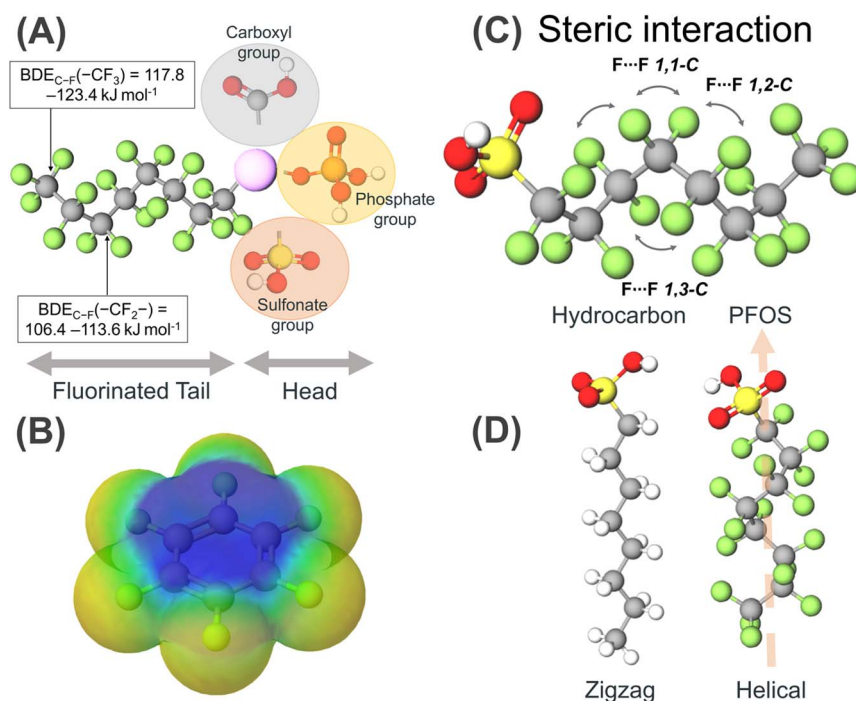

Fig. 1 (A) Representation of the structural properties of PFAS molecules having a fluorocarbon tail (BDE of the C−F bond for −CH$_3$ and −CH$_2$− groups are depicted) and a functional head group. The head group may vary from molecule to molecule, with the main functionalities, such as carboxylate, phosphate, and sulfonate groups. (B) Structure and electron density map of hexachlorobenzene, where the electron density is polarized towards the F groups having a reddish colour and the electron-deficient carbon backbone with blue colour. (C) Different types of F−F steric repulsion interaction between geminal, vicinal, and 1,3-substituted groups. (D) Comparison of structural dissimilarities of a PFAS and its hydrocarbon analogue, where the hydrocarbon shows the carbon backbone in a zig-zag structure, but owing to the enhanced steric repulsion in the PFAS molecules, the carbon backbone attains a helical structure.

8248 | J. Mater. Chem. A, 2025, **13**, 8246–8281

This journal is © The Royal Society of Chemistry 2025

a higher polarity than fluoromethane and trifluoro methane. Thus, introducing CF_2-type functionalities in molecules induces high polarity and low viscosity. The van der Waals radius of fluorine (1.47 Å) compared to hydrogen (1.20 Å) is large, resulting in steric congestion, and the substitution of all three fluorine atoms dramatically changes the conformation of PFAS molecules compared to their hydrocarbon analogues. Steric repulsions are also observed between the fluorine atoms relative to the 1,3 positions due to the formation of a helical structure (Fig. 1D). With an increase in the van der Waals radius from H to F, the C–C bond length of the carbon backbone gets stretched, and the C–C–C angle gets twisted by 12°, forming a helical structure with right and left helices in equal proportion, unlike the zig-zag conformation for hydrocarbons (Fig. 1C). Thus, PFAS are conformationally rigid molecules having less conformational freedom, which is attributed to the different steric constraints imposed by the presence of F groups.

Besides the tail part, they have a head group containing functionalities such as carboxylates, sulfonates, phosphates, amines, and many more (Fig. 1A). Owing to the strong electron-withdrawing nature of the perfluoroalkyl chains, the acidity of the OH groups is enhanced and the basicity of the organic functionalities present in the head group diminishes.[40] The increase in acidity is also attributed to the hyperconjugative stabilization by the β-fluorination. Thus, the pK_a values decrease when H atoms are replaced by F atoms in the alkyl chain. Despite the high electronegativity and lone pair over F, the low s and p orbitals are low-lying and relatively less polarizable, making them bad hydrogen bond acceptors. Thus, to study the sorption behaviour of PFAS, the pH of the solution becomes a crucial factor because it contains ionizable functional groups in protonated or deprotonated form. Functionalities such as carboxylic acid, phosphoric acid, phosphonic acid, and sulfuric acid show anionic character when they release H^+ ions in the solution. Cationic functionalities due to the presence of amines can accept H^+ from the solution or the presence of quaternary ammonium functionalities. Alternatively, zwitterionic PFAS consist of two or more of the above-mentioned functionalities. Lastly, there are few reported alcoholic PFAS, which do not ionize in aqueous solution, leading to the formation of non-ionic PFAS.[41]

PFAS are very weakly interacting *via* both intermolecular and intramolecular pathways owing to the low polarizability of their F groups, which are characterized by high volatility and low boiling compared to their hydrocarbon analogs. The lipophobic character of PFAS originates from their lack of van der Waals forces. These characteristics of PFAS pose severe challenges in selective sensing and remediation. The exceptionally low surface tension of PFAS is an attribute of the meager intermolecular forces between their interacting molecules.[42] Despite the high dipole moment of the CF_2 group, PFAS show a lower critical micellar concentration (CMC) (*i.e.*, the threshold concentration of PFAS molecules in solution above which they spontaneously form micellar aggregates) than their hydrocarbon counterparts, given that the dipole moments of the CH_2 groups cancel out each other in their helical chain structure, giving rise to non-polar and hydrophobic character.

PFAS form a unique fluorous phase *via* the creation of a phase boundary when encountering a mixture of polar and non-polar solvents, highlighting their amphiphilic character. Partitioning of fluorous materials resembling a biphasic separation process is driven by the free energy of the intermolecular interaction of PFAS in two phases.[43] This can be achieved by following two steps. The first step is the formation of a super-structure, where the consumption of energy leads to the assembly of PFAS molecules, further minimizing the surface tension. In this case, the required free energy depends on the interaction free energy of the PFAS molecules under self-assembly and the assembly size. In the second step, once the self-assembly is established, the molecules interact by van der Waals forces or other interactions such as H-bonding. This induces a change in physical properties with a change in the concentration of PFAS in the solution.

3. Classification of PFAS

PFAS can be classified based on their chain length, chemical structure, and functional groups attached to the carbon backbone. The detailed classification of PFAS is given below. Fig. 2 depicts a flowchart categorizing PFAS based on their carbon chain length, functional groups, and chemical structure.

3.1. Classification of PFAS based on carbon chain length

The categorization of PFAS according to their carbon chain length is critical for understanding their environmental destiny, toxicity, and possible effects on human health and the ecosystem.[44]

Generally, short-chain PFAS are comprised of perfluoroalkyl chains with fewer than six carbon atoms. Short-chain PFAS include perfluorobutanesulfonic acid (PFBS), perfluoropentanoic acid (PFPeA), perfluorohexanoic acid (PFHxA), and perfluoroheptanoic acid (PFHpA). Long-chain PFAS are composed of perfluoroalkyl chains containing six or more carbon atoms. Due to their distinct features, such as oil and water repellency, thermal stability, and surfactant capabilities, these compounds are widely employed in various industrial and consumer applications.[1,21] Long-chain PFAS include perfluorooctanoic acid (PFOA), perfluorooctanesulfonic acid (PFOS), perfluorononanoic acid (PFNA), and perfluorodecanoic acid (PFDA). Concerns regarding the environmental persistence and bioaccumulation of long-chain PFAS have led to the use of alternative compounds.[45,46] Short-chain PFAS are thought to have lower bioaccumulation potential and shorter environmental persistence than long-chain PFAS.[45,47,48] Long-chain PFAS are known to have higher bioaccumulation capacity and longer environmental persistence than short-chain PFAS.[45,47,48]

3.2. Classification of PFAS based on chemical structure

3.2.1. Linear PFAS. Linear PFAS have straight-chain perfluoroalkyl groups. The carbon atoms in these fluorinated chains are arranged linearly. Linear PFAS may have distinct chemical and physical characteristics depending on the length of their perfluoroalkyl chain. Linear PFAS include
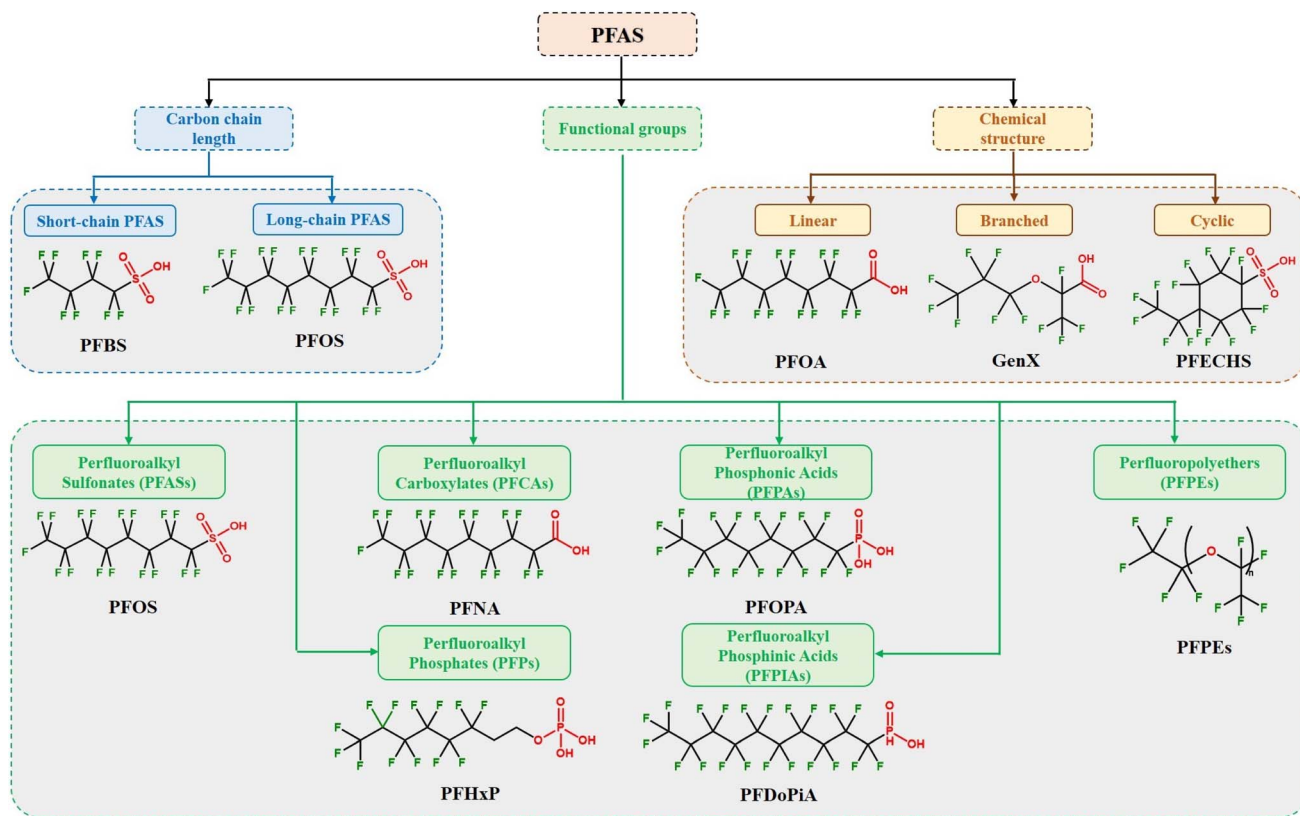
Fig. 2 Classification of PFAS based on carbon chain length, functional groups, and chemical structure with examples.

perfluorooctanoic acid (PFOA) and perfluorooctanesulfonic acid (PFOS).

3.2.2. Branched PFAS. Perfluoroalkyl chains with branching points give branched PFAS their non-linear structures. Their chemical and physical characteristics may be influenced by branching. Thus, branched PFAS may show different solubility, reactivity, and environmental destiny than their linear counterparts. Certain perfluorocarboxylic and perfluorosulfonic acids are examples of branched PFAS.

3.2.3. Cyclic PFAS. Perfluoroalkyl chains organized in rings or cycles make up cyclic perfluoroalkyl substances (PFAS). The existence of ring structures in these compounds may give rise to unique characteristics such as enhanced stiffness and conformational flexibility. Compared to linear or branched PFAS, cyclic PFAS may exhibit distinct environmental behaviors and toxicological profiles. Perfluoropolyethers (PFPEs) and several perfluoroalkyl phosphonic acids are examples of cyclic PFAS.

The chemical structure-based categorization of PFAS sheds light on the variety of these substances as well as their possible characteristics and behaviors. It is essential to comprehend the structural properties of perfluoroalkyl substances (PFAS) to predict their destiny in the environment, evaluate their toxicity, and create mitigation plans that work.

3.3. Classification of PFAS based on functional groups

3.3.1. Perfluoroalkyl sulfonates (PFASs). PFASs are composed of a perfluoroalkyl chain with an attached sulfonate

($-SO_3^-$) functional group. These substances have excellent heat stability and potent surfactant qualities. PFASs are often utilized in industrial settings as coatings, firefighting foams, and surfactants. Perfluorooctanesulfonic acid (PFOS) and perfluorobutanesulfonic acid (PFBAS) are two examples of PFASs (PFBS).

3.3.2. Perfluoroalkyl carboxylates (PFCAs). A perfluoroalkyl chain is joined to a carboxylate ($-COO-$) functional group in PFCAs. Due to their chemical stability and surfactant qualities, these compounds are widely employed in various consumer and industrial applications. PFCAs are frequently discovered in the environment as pollutants and show modest thermal stability. Perfluorooctanoic acid (PFOA) and perfluorononanoic acid (PFNA) are two examples of PFCAs (PFNA).

3.3.3. Perfluoropolyethers (PFPEs). PFPEs possess ether linkages ($-O-$) in their perfluoroalkyl chain. These substances are known for having strong chemical and thermal stability as well as outstanding lubricating qualities. PFPEs are often utilized in a variety of industrial applications as hydraulic fluids, lubricants, and heat transfer fluids. Grease and oils made of perfluoropolyether are examples of PFPEs.

3.3.4. Perfluoroalkyl phosphonic acids (PFPAs). A perfluoroalkyl chain is joined to a phosphonic acid ($-PO(OH)_2$) functional group in PFPAs. These substances have strong solubility in polar liquids and work well as corrosion inhibitors. Applications needing corrosion protection, such as surface treatment and metal plating, employ PFPAs.

8250 | J. Mater. Chem. A, 2025, 13, 8246–8281

This journal is © The Royal Society of Chemistry 2025

Perfluorooctylphosphonic acid (PFOPA) and perfluorodecylphosphonic acid (PFDoPA) are two common PFPAs.

3.3.5. Perfluoroalkyl phosphinic acids (PFPIAs). A perfluoroalkyl chain is joined to a phosphinic acid (–PO(OH)) functional group in PFPIAs. These substances are efficient metal ion sequestrants with potent chelating properties. PFPIAs are used in chemical synthesis, wastewater treatment, and metal extraction, among other sectors. Perfluorooctylphosphinic acid (PFOPiA) and perfluorodecylphosphinic acid (PFDoPiA) are two examples of PFPIAs.

3.3.6. Perfluoroalkyl phosphates (PFPs). A perfluoroalkyl chain is joined to a phosphate (–PO₄) functional group in PFPs. Due to their excellent flame resistance, these substances are utilized as flame retardants in textiles and polymers. PFPs are also utilized in specialized applications such as lubricants and hydraulic fluids. Perfluorooctylphosphate (PFOP) and 2-(perfluorohexyl) ethanol phosphate (PFHxP) are two examples of PFPs.

Functional group-based PFAS categorization sheds light on the chemical makeup, uses, and environmental characteristics of these substances. To evaluate the environmental destiny of PFAS and their toxicity and possible threats to the ecosystem and human health, it is essential to comprehend the various functional groups present in these substances.

4. Traditional PFAS detection methods and their limitations

PFAS detection has been performed using chromatographic techniques such as liquid chromatography-mass spectrometry (LC-MS), liquid chromatography-mass spectrometry/mass spectrometry (LC-MS/MS), gas chromatography-mass spectrometry (GC-MS), ultra-high-performance liquid chromatography (UHPLC), and HPLC.[49] The LC-MS/MS technique has long been established as the gold standard for PFAS detection due to its remarkable sensitivity, accuracy, and reliability.

Methods 533, 537, and 537.1, certified by the Environmental Protection Agency (EPA), are essential for identifying PFAS and providing standardized procedures for tracking these enduring pollutants.[50–52] Solid-phase extraction (SPE) utilizing a polystyrene-divinylbenzene (SDVB) resin is used in Method 533. Subsequently, LC-MS/MS, equipped with a C18 column, is utilized for analysis to provide enhanced column efficiency and analyte resolution in shorter run times. This technique has been useful in measuring PFAS in various aqueous media, including drinking water, with LOD in the range of 1.4 to 16 parts per trillion (ppt) for twenty-five analytes. However, the drawbacks of using this analytical method include its 35 min minimum run time and sole focus on analyzing drinking water samples. The solid-phase extraction methodology with LC-MS/MS investigation is shared by Method 537, an expansion of Method 533, which enables the measurement of 29 PFAS. Although it effectively identifies PFAS in drinking water, it is primarily designed for a given matrix and has the same time constraint of 35 min as Method 533. Aiming to improve the analytical procedures, Method 537.1 has been refined in

response to these restrictions. Method 537.1 reports reduced detection limits ranging from 0.71 to 2.8 ppt, with an emphasis on eighteen PFAS analytes. Its primary focus, similar to that of its predecessors, is on drinking water analysis, which highlights the necessity for wider application to a variety of matrices such as soil, food, and air.

Although not recommended by the EPA, other research groups have presented multiple modifications to these approaches. For instance, dispersive solid-phase extraction (d-SPE) was used to assess the quantity of PFOA and PFOS in honey samples.[53] Up to 87% of the sample was recovered and subjected to micro-ultrahigh performance liquid chromatography (UHPLC)-MS/MS analysis. The d-SPE technique distinguishes itself from SPE cartridges, which may face clogging issues when extracting a contaminated matrix. In contrast, the d-SPE method employs a minimal quantity of sorbents dispersed in an aqueous solution. This approach ensures efficient compound recovery and minimizes the solvent usage, while optimizing the utilization of the sorbent surface area.[54] Therefore, more research on d-SPE for PFAS analysis in various water matrices should be conducted. Another quick and easy analytical technique was reported for analyzing perfluorocarboxylic acids (PFCAs) in water medium at small concentrations.[55] This study used tetrabutylammonium (TBA) as an ion pair in combination with solid phase micro extraction (SPME), followed by in-port derivatization-GC-negative ion chemical ionization MS. This method was recommended for the quick screening of PFCAs in ecological matrices given that involves shorter analytical times, smaller sample and solvent volumes, and better recoveries.

To fully comprehend the fate and transit of fluorinated compounds, especially PFAS, in the environment, it is imperative to close the fluorine mass balance.[56] Researchers may ascertain the presence and distribution of PFAS in the environment by utilizing the above-mentioned conventional analytical methods and their modifications. Fig. 3 provides an outline of the analytical techniques that may be applied to close the fluorine mass balance. The fluorine mass balance can help us understand the mechanisms by which PFAS enter, migrate through, and depart environmental compartments by considering all sources, sinks, and transformations of these chemicals. This knowledge is essential for evaluating the possible concerns connected to the presence of PFAS, such as their persistence, bioaccumulation, and possible negative impacts on ecosystems and public health. Closing the fluorine mass balance also makes it possible to pinpoint information gaps and create more precise prediction models for the behavior of PFAS in the environment, which helps with the creation of efficient management plans to lessen their effects.

Although the EPA-approved methods and their modifications have been instrumental in detecting PFAS, their drawbacks, such as the time-consuming nature of the analysis and matrix specificity, highlight the need for more sophisticated sensor approaches. Also, the issue of peak separation with PFOA and PFOS in chromatographic systems is one of the most well-known drawbacks. This is because the blank comes from common polymeric materials, which means that PFOA may be

This journal is © The Royal Society of Chemistry 2025

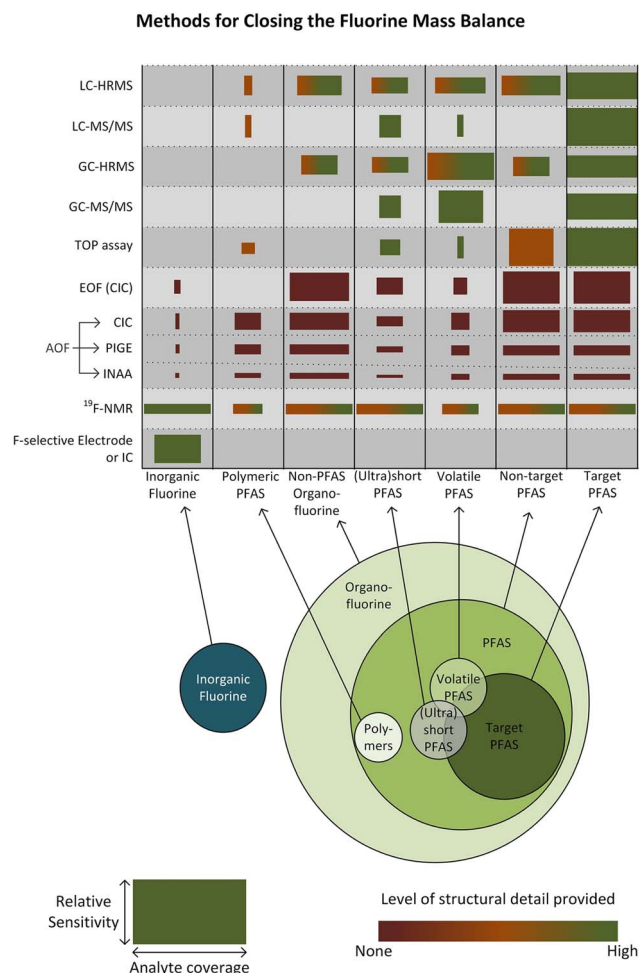J. Mater. Chem. A, 2025, **13**, 8246–8281 | **8251**

Fig. 3 Outline of the analytical techniques that may be applied to close the fluorine mass balance in PFAS. The widths of the boxes show the general coverage of the technique within the appropriate category of fluorinated chemicals, and the heights indicate the general sensitivity of the method. Reproduced from ref. 56 Copyright 2024, ACS.

maintained and eluted after the injected PFOA.[57] Only volatile, semi-volatile, and neutral PFAS can be detected by gas chromatography (GC) and requires a combination of electron impact (EI) or chemical ionization (CI) to provide the benefit of mass spectral library application, which limits its applicability and makes it less common than LC.[8] Nevertheless, the LC-MS method has drawbacks comparable to that of the GC-MS technique, including the need for lengthy sample analysis and high costs (average cost of $400 per sample analysis) for typical environmental monitoring applications.[58] It is essential to have rapid, portable, affordable, and easy-to-use detection techniques to fulfill the increasing need for thorough PFAS monitoring in a range of environmental settings.

A promising strategy to circumvent the limitations of existing technologies is to use advanced nano-sensors composed of newly developed nanomaterials and sensing processes. This will ensure that PFAS can be detected effectively and widely outside standard laboratory settings with better LOD and improved precision.

5. Nano-sensors for PFAS detection

A wide range of 0D, 1D, 2D, and 3D nanomaterials, both organic and inorganic, has unique physiochemical characteristics and can be used to fabricate sensors for detecting PFAS and other organic contaminants.[59,60] These nanoparticles are vital components that provide a diverse framework for customizing the performance of sensors.[61,62] The categorization of PFAS sensors is inextricably tied to their underlying processes with materials and output signals (Fig. 4). Optical sensors use nanomaterials with various optical characteristics to modulate light signals to detect PFAS. Surface-enhanced Raman scattering (SERS) sensors, made possible by nanomaterials, use increased Raman signals to detect PFAS with greater specificity. Electrochemical sensors, which use nanomaterials with good electrocatalytic capabilities, provide quantitative signals indicative of PFAS concentrations via electrochemical processes. Immunosensors are based on functionalized nanomaterials, which allow the selective binding of PFAS to antibodies on nanomaterial surfaces, resulting in measurable signals. Microfluidic sensors incorporate nanoparticles into microfluidic systems, providing accurate and regulated PFAS detection, while also increasing the overall efficiency and speed in sensing operations. This comprehensive viewpoint highlights the critical significance of nanomaterials in several sensor modalities for PFAS detection, stressing their subtle contributions to sensor design and operation.

5.1. Optical PFAS nano-sensors

Optical nano-sensors are an innovative class of sensing devices that use the unique features of nanomaterials to detect and analyze a wide range of chemicals at the nanoscale. These sensors use optical principles to detect light–matter interactions very sensitively and selectively.[63] Nanomaterials, including nanoparticles, quantum dots, and nanocomposites, are crucial in improving the optical characteristics of these sensors. Colorimetry, fluorescence, plasmonics, and surface-enhanced Raman spectroscopy (SERS) are all methods used by optical nano-sensors. The inclusion of nanomaterials enables fine control of the sensor parameters, allowing customized responses to specific analytes. In the context of PFAS detection, optical nano-sensors have benefits such as fast reaction times, high sensitivity, and real-time operation. Optical nano-sensors are promising technology at the vanguard of advanced sensing platforms because of their adaptability in various applications, ranging from complex medical diagnostics to environmental monitoring.

5.1.1. Colorimetric PFAS nano-sensors.
Nanomaterials that change color in the presence of a target, such as a specific molecule or ion, are commonly employed in colorimetric sensors. The analyte concentration is connected with the change in hue to generate an easy and visible readout. A detailed examination of optical sensors employing gold nanoparticles (AuNPs) designed for sensing anionic pollutants was reported, specifically considering PFOS and PFOA.[64] Various optical sensors were constructed, employing AuNPs as the

8252 | J. Mater. Chem. A, 2025, 13, 8246–8281

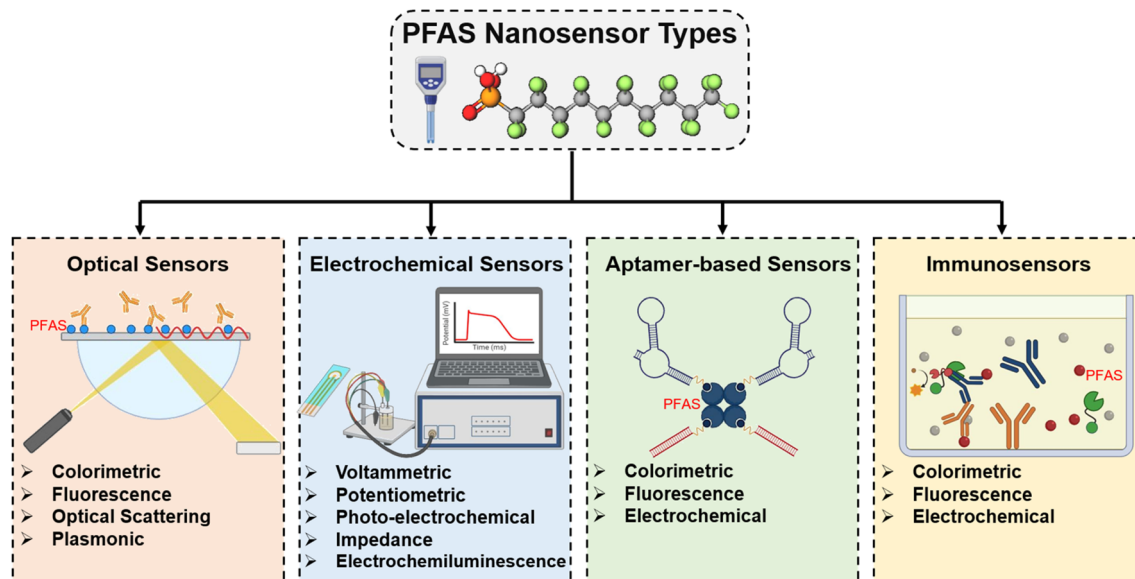This journal is © The Royal Society of Chemistry 2025

Fig. 4 Types of PFAS nano-sensors based on the underlying processes with materials and output signals.

experimental basis for anions. The identification process for the targeted anions involves induced aggregation, binding of anions, release (of dye or other substances), and etching of AuNP (Fig. 5A). The functionalization of AuNPs in these sensors involved employing thiol-terminated polystyrene or monolayers of alkane thiolates terminated with poly(ethylene glycol) (PEG-thiol) and perfluorinated thiols (F-thiol). In the former configuration, PFOA dislocates the polystyrene ligands by attaching them to the AuNPs, leading to their aggregation through

fluorine–fluorine (F–F) interactions. This aggregation induces a discernible color shift from red to blue-purple. Notably, the observed color change is perceptible to the naked eye, albeit with a detection threshold above 103 ppm, a comparatively elevated concentration. The authors proposed the potential for color-changing aggregation induced by perfluorinated carboxylic acids (PFCAs) as a broader class. In the latter sensor design, the F-thiol functionalization facilitates the binding of PFAS *via* F–F interactions, ensuing in the precipitation of AuNPs from the solution. With an increase in PFAS concentration, the red color intensity of the reaction media diminishes. This color modulation is observable and quantifiable through visual inspection and spectroscopy. Due to the inherent affinity of PFAS for the F–F interaction, the sensor can detect multiple PFAS species with different functional moieties, although short-chain PFAS (<C7) display reduced sensitivity, which is attributed to their decreased hydrophobicity. Remarkably, this sensor achieved a detection limit as low as 10 ppb for long-chain PFAS (>C7).

In another study, MoS_2/Fe_3O_4 nano-flowers were employed as a platform for the colorimetric detection of PFAS due to their inherent peroxidase-mimicking and electroactive properties, which could produce a blue hue when 3,3,5,5-tetramethylbenzidine (TMB) was oxidized with H_2O_2, as illustrated in Fig. 5B.[65] The recognition mechanism involves electrostatic interactions and hydrogen bonding between the hydroxyl groups of the Fe_3O_4 nanoparticles and the sulfonate groups of PFOS. Additionally, the steric hindrance effect resulting from the spatial arrangement of these moieties contributed to the excellent specificity of this sensor. To assess the specificity of the sensors, various target chemicals, including analogs of PFOS such as octanoic acid (OA), decanoic acid (DA), dodecanoic acid (DDA), dodecanediol, 1-dodecyl amine, sodium dodecyl sulfate (SDS), sodium dodecyl benzene sulfonate (SDBS), cetyltrimethylammonium bromide (CTAB), sodium octadecanesulfonate, and 1-hexadecane sulfonate (SHDS), were
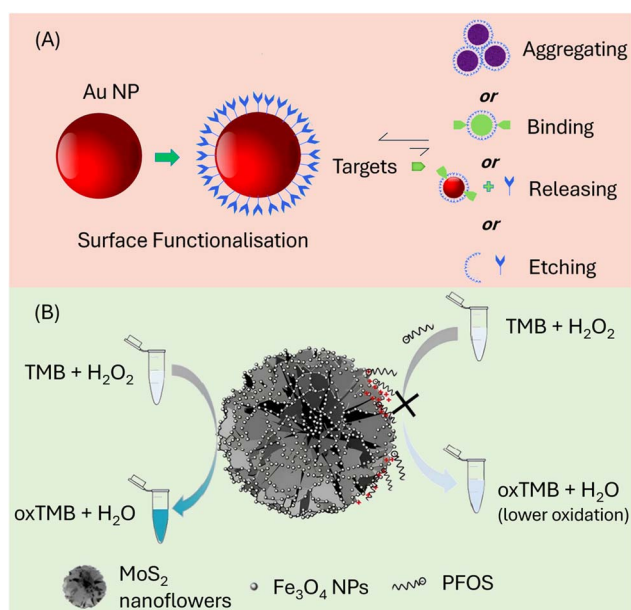

Fig. 5 (A) Illustration of the possible interactions between Au NPs and the target analyte. Reproduced from ref. 64 Copyright 2017, Elsevier. (B) MoS_2/Fe_3O_4 nano-flowers for the colorimetric determination of PFAS producing a blue hue when 3,3,5,5-tetramethylbenzidine (TMB) is oxidized in H_2O_2. Reproduced from ref. 65 Copyright 2019, Elsevier.

introduced as interferences during the detection. The recovery rate for these interfering substances in river and tap water samples was found to be ~85%. This underlines the robustness and applicability of the MoS_2/Fe_3O_4 nano-flower-based sensor for the detection of PFAS in complex environmental samples. Table 1 represents the attributes of the reported optical PFAS nano-sensors.

Colorimetric PFAS nano-sensors have benefits such as quick and visually perceptible detection, making them a natural choice for the on-site monitoring of PFAS. The detection levels may vary depending on the specific targeted PFAS compounds and the sensor design but commonly fall in the range of 1 to 100 $\mu g\ L^{-1}$. These sensors frequently have excellent sensitivity, allowing them to detect tiny concentrations, and their simplicity allows user-friendly applications that do not require complicated equipment. However, the possibility for interference from compounds with comparable color-changing capabilities limits the specificity of colorimetric PFAS nano-sensors in complicated sample matrices. Furthermore, they may impose detection thresholds because they rely on observable color changes, making them less suited for ultra-trace PFAS levels. Furthermore, colorimetric sensors may lack the quantitative precision of more complex analytical techniques, making it challenging to detect PFAS concentrations correctly. Quantitatively, the precision of colorimetric sensors may vary, with detection errors typically falling in the range of ±10% to ±50%, depending on factors such as sensor design, calibration, and environmental conditions.

5.1.2. Fluorescence PFAS nano-sensors. To detect PFAS, fluorescence-based PFAS nano-sensors use the concept of "turn on" or "turn off" procedures. The presence of PFAS causes a considerable increase in fluorescence intensity in the "turn on" configuration, generally due to the particular binding or interaction between PFAS and the nanomaterials or displacement of fluorophores, resulting in a perceptible and quantitative signal augmentation. In contrast, in the "turn off" mechanism, the fluorescence intensity decreases following PFAS engagement, often due to quenching effects or formation of a complex, allowing sensitive and selective PFAS detection with detection limits ranging from ng L^{-1} to $\mu g\ L^{-1}$ depending on the specific nanomaterial used, experimental conditions, and detection method employed, via deviations in the emission characteristics of fluorescent nanomaterials (Fig. 6A). These technologies provide flexible approaches for constructing very sensitive and selective PFAS sensors based on fluorescence responses.

Using a surface molecular imprinting approach, Feng and colleagues created a fluorescence sensor for perfluorooctane sulfonate (PFOS, $C_8F_{17}SO_3$).[72] A molecularly imprinted polymer (MIP) was immobilized onto SiO_2 NPs throughout this procedure. A hybrid monolayer consisting of a covalently anchored fluorescent dye and organic amine was generated on the surface of MIP-SiO_2 NPs under acidic conditions (pH 3.5), functioning as receptor sites for $C_8F_{17}SO_3$ via acid–base pairing and hydrogen-bond interactions. The fluorescence quenching was caused by electron transfer between the fluorescent dye and PFOS, which was enhanced by the selective binding of PFOS

Table 1 Attributes of various colorimetric PFAS nano-sensors reported

Optical sensor types	Platform nanomaterial	Receptor/probe	Target analyte	Mechanism/PFAS interaction	Range ($\mu g\ L^{-1}$)	LOD ($\mu g\ L^{-1}$)	Ref.
Colorimetry	Au NPs	PEG-thiols and PFAS terminated (F thiols) alkanethiols modified Au NPs (Au@PEG-F NPs)	PFOA, PFOS, PFBS, PFHxS, PFHpA, PFNA, PFTrDA, PFTeDA, PFHxDA, PFODA	Color change and SPR peak shift in UV-visible spectra	10^2–10^4	100	66
	Fe_3O_4 NPs	3D magnetic MoS_2/Fe_3O_4 nanoflowers	PFOS	Hydrogen bonding between the hydroxyl groups of the Fe_3O_4 NPs and the sulfonate groups of PFOS and steric hindrance causes electrostatic contact	50.01 to 6251.58	4.3	67
	Au NPs	Poly(styrene)-coated Au NPs	PFOA, tridecafluoroheptanoic acid	F–F interactions are used to aggregate Au NPs	1.04–2.07×10^5	104 000	68
	Carbon dots (CDs)	—	PFOS	Ground-state complex formation between CDs	0.5–8	7.587×10^{-2}	69
	MOFs-derived Co–N–C nanosheets (CoNCN)	3,3′,5,5′-Tetramethylbenzidine (TMB)	PFOS	The oxidase-mimicking property of CoNCN due to $\cdot$OH, O^{2-} and $_1O^2$ oxidize TMP (oxTMB), and the addition of PFOS fade the blue color of oxTMB	0.01 to 100	0.02	70

8254 | J. Mater. Chem. A, 2025, **13**, 8246–8281

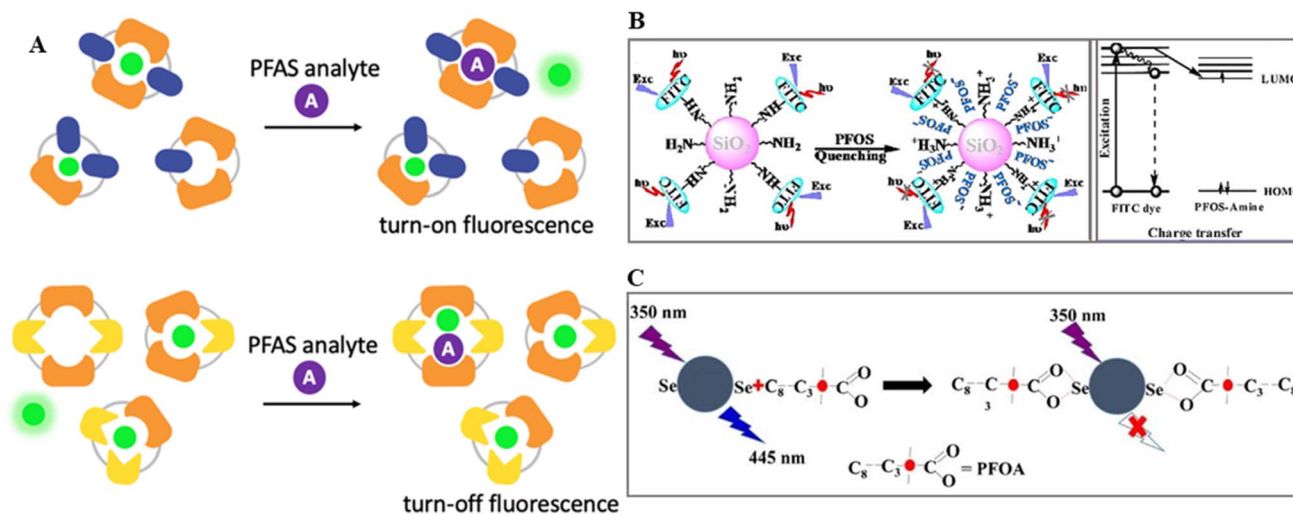This journal is © The Royal Society of Chemistry 2025

Fig. 6 (A) Illustration of the two possible mechanisms of fluorescence manipulations either by releasing fluorophores or forming a ternary complex with the fluorophore, receptor and PFOs. Reproduced from ref. 71 Copyright 2023, the Royal Society of Chemistry. (B) Schematic of turn-off sensing of PFOS anions *via* energy and charge transfer channels by MIP-SiO$_2$ NPs. Reproduced from ref. 72 Copyright 2014, Elsevier. (C) Schematic of the interaction between SeN–CDs and PFOA for fluorescence quenching turn off sensing. Reproduced from ref. 73 Copyright 2019, Springer.

within the recognition cavities of the polymer matrix. Surface-anchored primary amino ligands incorporated into SiO$_2$ NPs with molecularly imprinted polymer (MIP) caps acted as recognition elements. These ligands engaged PFOS through robust acid–base and/or hydrogen-bond interactions. Upon rebinding to the recognition cavities, the PFOS anions quenched the fluorescence emission of the FITC dye *via* energy and charge transfer pathways (Fig. 6B). The effectiveness of this quenching process is correlated with the binding affinity of PFOS to the surface of MIP-capped NPs. The proposed method demonstrated the precise and selective detection of PFOS in water, achieving a detection limit as low as 5.57 µg L^{-1}. The linear relationship extended across the concentration range of 5.57–48.54 µg L^{-1} (corresponding to 10.36–90.2 nM).

Carbon dots (CDs) are widely explored fluorescent nano-materials in the ratio-fluoro-metric sensing of organic and inorganic analytes.[74] A fluorometric approach was proposed for the detection of PFOA employing CDs co-doped with selenium and nitrogen (SeN-CDs) as a fluorescent platform, where complex formed between SeN-CDs and PFOA showed rational quenching (turn off).[73] This method is suitable for the quantitative aqueous sensing of PFOA in the range of 10–70 M with an LOD of 1.8 M. The combination of SeN-CDs and PFOA is shown in Fig. 6C. Because carboxylate and fluorocarbon groups are hydrophilic and hydrophobic, respectively, PFOA molecules tend to adsorb on hydrophilic surfaces and interact with nearby surface carboxylate groups *via* complexation. "Selenium has electron affinity to receive electrons because of its comparatively high electronegativity value, whereas fluorine in PFOA has an even greater electronegativity to draw electrons from surrounding groups. Given that SeN-CDs are extremely soluble, PFOA molecules can spontaneously reach the surface of the nanoprobes and form complexes *via* carboxylate groups based on hydrophilic attraction. Additionally, surface Se-containing

groups tend to donate electrons to PFOA".[73] This results in the formation of an SeN-CD-PFOA complex. Thus, the internal electron transfer in the chelation complex accounts for the observed quenching and shorter lifetime.

In another investigation, the fluorescent turn-on visual sensing of PFOS utilizing blue fluorescent CDs and berberine chloride hydrate (BH) was proposed.[75] It was observed that when BH was introduced in pH 6.09 Britton–Robinson (BR) buffer solution, the fluorescence of CDs decreased. No other perfluorinated molecule caused the fluorescence to be partially restored (turned on) at 448 nm, which seemed to increase at 533 nm when PFOS was introduced. PFOS/PFOA did not impair the fluorescence of the CDs. However, PFOS boosted the fluorescence intensity of BH. This showed that fluorescence amplification in the CD-BH system occurs due to the interaction between BH and PFOS when PFOS is present. Alternatively, the CD-BH-PFOS solution has a more significant visualization impact (higher identification by the naked-eye) than the BH-PFOS system (colorless to yellowish green). Table 2 presents the attributes of the reported fluorescence PFAS sensors.

Fluorescence-based PFAS nano-sensors have several benefits, including excellent sensitivity with detection specificity often exceeding 90% for targeted PFAS compounds, enabling the detection of trace amounts of PFAS with great accuracy. These sensors frequently give real-time and quantitative results, allowing the detection of PFAS across a wide dynamic range. However, their drawbacks include the possibility of interference from complicated sample matrices, which may impair the sensor specificity, and the need for specialized equipment, increasing the total cost and complexity of the detection system. For example, different organic and inorganic chemicals may interfere with the fluorescence signal in complex environmental samples such as wastewater and soil extracts, resulting in false-positive or false-negative findings. Furthermore, the

This journal is © The Royal Society of Chemistry 2025

J. Mater. Chem. A, 2025, **13**, 8246–8281 | **8255**

Table 2 Attributes of various reported fluorescence and optical scattering PFAS nano-sensors

Optical sensor types	Platform nanomaterial	Receptor/probe	Target analyte	Mechanism/PFAS interaction	Range (μg L^{-1})	LOD (μg L^{-1})	Ref.
Fluorescence	SiO$_2$ NPs	FITC dye-NH$_2$-APTS MIP	PFOS	Direct fluorescent recognition	5.57–48.54	5.57	72
	Carbon dots (CDs)	Berberine chloride hydrate (BH)	PFOS	In BR buffer solution, BH quenches (turn off) fluorescence of CDs and PFOS restored their fluorescence (turn on)	110.028–25 006.3	10.853	75
	Magnetic iron oxide nanoparticles	Guanidinocalix[5]arenes	PFOS, PFOA	Molecular van der Waals forces between electron-deficient GC5A-6C and the e-rich sulfonate head group of PFOS, as well as hydrogen bonding between guanidium groups of GC5A-6C and the PFOS head group, leading to fluorescence enhancement (turn on)	50–4000 (PFOS); 100–1000 (PFOA)	11.3 $\pm$ 0.2 (PFOS); 10.9 $\pm$ 0.1 (PFOA)	76
	N-Doped carbon dots (N-CDs)	Ethidium bromide	PFOS	Through electrostatic interaction and hydrogen bonding, N-CDs can react with negatively charged PFOS, causing aggregation and fluorescence quenching (turn off) and an increase in SOS, a scattering light signal	0–1000.25	13.9	77
	Chitosan doped CDs	Epichlorohydrin	PFOS	The sulfonate group of PFOS can complex with the amino group via hydrogen bonding or electrostatic reactions, enhancing the conjugation degree of H$_2$N-passivated CQDs and leading to enhanced fluorescence emission (turn on)	2×10^{-5}–2×10^{-4}	4×10^{-7}	78
	CDs	—	PFOS, PFOA	Electron transfer mechanism and fluorescence quenching (turn off)	3×10^{-3}–16 (PFOS); 0.05–1 (PFOA)	5×10^{-3} (PFOS); 1×10^{-2} (PFOA)	79
	CDs	—	PFOS	CD-PFOS ground-state complex formation, leading to static quenching (turn off)	0.2–12	1.827×10^{-2}	69
	NaYF4 UCNPs	Perfluorooctyltriethoxysilane-functionalized tricolor probes	PFOS, PFOA, PFDA, PFNA, PFHpA, PFHxA, PFHxS	Hydrogen bonding between probes and PFOS, fluorescence quenching (turn off) due to charge/energy transfer between the SiO$_2$ layer and PFOS	—	20.005	80
	QDs	Chitosan MIP	PFOS	Fluorescence quenching (turn on)	20–200×10^{-6}	60×10^{-6} (serum); 85×10^{-6} (urine)	78
	Covalent organic frameworks	Lanthanide-doped nanocrystals	PFOS	Through hydrogen bonds or electrostatic interactions, the PFOS sulfonate groups interact with the amino groups and the hydrogens on the benzene ring of the COFs and quench the fluorescence (turn on)	90.02×10^{-6}	75.02×10^{-6}	81
	CdS quantum dots	3-Mercaptopropionic acid (MPA)	PFOA	Aggregation-dispersion of MPA-CdS-QDs results in fluorescence quenching (turn off)	200–16 000	120	82
Optical scattering	AgNPs on silicon	Dye-ethyl violet or methyl blue and graphene oxide coating	PFOA	Surface-enhanced Raman scattering	50–500	50	83
	CDs	—	PFOS	Resonance light scattering	0.5–12	1.2045	69

8256 | J. Mater. Chem. A, 2025, **13**, 8246–8281

This journal is © The Royal Society of Chemistry 2025

photobleaching of fluorophores and sensitivity to environmental conditions may cause difficulties in maintaining the stability of the sensor over long periods.

5.1.3. Optical scattering PFAS nano-sensors. PFAS nano-sensors based on optical scattering involve the use of several methods such as Raman scattering, Rayleigh light scattering, resonance light scattering, and resonance shift to provide sensitive PFAS detection and quantification. For instance, Rayleigh light scattering methods may identify PFAS compounds at concentrations as low as 0.1 ng L^{-1}, whereas Raman scattering techniques can detect them as low as 1 ng L^{-1}. Even higher sensitivity is possible using resonance shift and resonance light scattering methods, which have detection limits as low as 0.01 ng L^{-1} for certain PFAS species. When incoming photons interact with PFAS molecules in Raman scattering, specific frequency changes in the scattered light correlate with the rotational and vibrational transitions in the molecules.[84] PFAS nano-sensors monitor these optical scattering events to identify molecular interactions, enabling accurate and targeted PFAS sensing in diverse complex matrices. When the wavelengths of Rayleigh scattering and molecule absorption coincide, a particular type of light scattering known as resonance light scattering (RLS) occurs. This resonance, which is seen when incoming light interacts with specific molecules, strengthens the scattering signal. Rayleigh light scattering and resonance shift-based PFAS nano-sensors have not been reported to date. There is not much evidence of advancements using these particular sensing approaches in the research landscape in this field. However, there are a few reports on PFAS nano-sensors using SERS, suggesting some advancement in alternative sensing techniques.

The PFAS, metal surface distance, particle orientation, and conformation affect SERS and the shape, size, and assembly of metallic nanoparticle (MNP). The intensity of the interaction between the PFAS and MNP determines the signal enhancement. As seen in Fig. 7A, the Raman intensity changes with the location of the analyte. The position of the analyte determines the Raman intensity, where at position 1, there is minimal Raman scattering due to the negligible electromagnetic charge transfer external to the metal surface; at position 2, charge transfer with MNP results in a weak Raman spectrum; and at position 3, significant electromagnetic charge transfer causes enhanced Raman scattering, which is known as a hotspot and is attributed to localized surface plasmon resonance (LSPR) effects.

Fang and colleagues used SERS methods to identify firefighting foams, essential sources of PFAS in the environment.[83] They obtained an LOD of 50 ppb for perfluorooctanoic acid (PFOA) using two SERS substrates, namely, nanosphere lithography Ag and graphene oxide (GO) membrane, loaded with dye-fluoro surfactant (FS) precipitate ion pairs. The adsorption of certain PFAS compounds was aided by adding Si–Ag–GO membranes with flat surfaces. The experiments under controlled conditions showed that adding a dye, such as ethyl violet, considerably enhanced the loading capacity of FS on the GO surface. Using various colors, the replacement of perfluorooctanesulfonic acid (PFOS) with PFOA and modifications
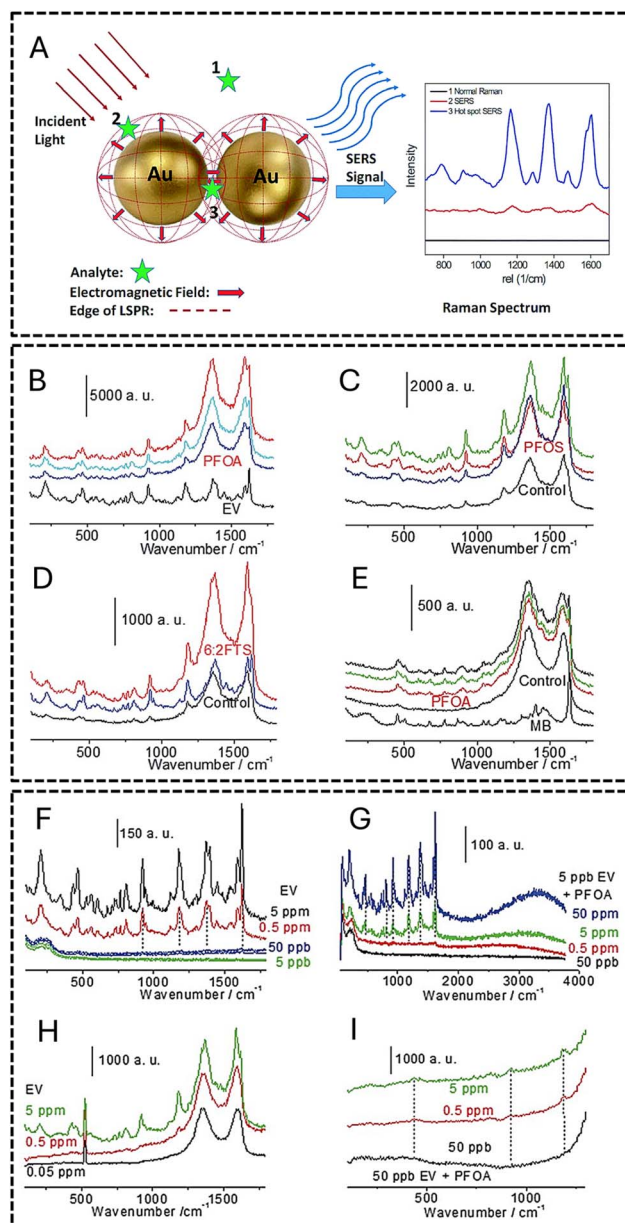

Fig. 7 (A) Schematic of surface-enhanced Raman scattering (SERS) sensing of an organic analyte on AuNPs. Reproduced from ref. 85 Copyright 2015, the Royal Society of Chemistry. (B–I) Raman spectral analysis of the assembly of dye–FS–GO; LOD of the assembly of dye–FS–Ag (J and K) and dye–FS–GO (H and I). Reproduced from ref. 83 Copyright 2016, the Royal Society of Chemistry.

to the ion-pair components were investigated, offering insights into the SERS substrate detection capabilities. Dye–FS–Ag and dye–FS–GO LOD assemblies were observed, where the latter had a 50 ppb LOD. The silicon peak at 512 cm^{-1} was used as the reference for the GO membrane. The Raman spectrum analysis of the dye–FS–GO and dye–FS–GO LOD incubation assemblies is displayed in Fig. 7B–I. Table 2 represents the attributes of the reported optical scattering PFAS sensors.

One of the advantages of SERS is its adjustable surface, allowing improved detection using direct and indirect

This journal is © The Royal Society of Chemistry 2025

J. Mater. Chem. A, 2025, **13**, 8246–8281 | **8257**

methods.[86] Furthermore, the adaptability of this technology enables the creation of nano-sensors with various uses. Nevertheless, there are obstacles to overcome, such as the difficulty of fabricating substrates, the possibility of signal fluctuation due to external factors, and the related expense of creating highly reproducible SERS substrates. These issues must be resolved for SERS-based PFAS nano-sensors to be widely used in practical applications.

5.1.4. Plasmonic PFAS nano-sensors. Plasmonics plays a significant role in the development of PFAS nano-sensors. AuNPs and AgNPs are often used in the detection of PFAS using plasmonic nano-sensors.[87] These nano-sensors use the distinctive optical features of AgNPs and AuNPs, such as surface plasmon resonance (SPR). SPR is an aspect of sensing that uses variations in refractive index close to a metal surface. Surface plasmons are excited when polarized light strikes a metal surface at a particular angle, causing the surface plasmon phenomenon. SPR is used to detect PFAS and other pollutants in various sensor platforms, such as optical fibers and nanoparticles.[58] In recent advancements, utilizing SPR in conjunction with nanostructures and molecularly imprinted polymers (MIPs) has improved the sensitivity and selectivity, with detection limits as low as pg mL^{-1} for a variety of target analytes.[88]

MIP was deposited on a D-shaped plastic optical fiber (POF) shielded with a photoresist buffer layer and a thin Au film.[89] To generate this optical platform, the POF cladding was removed (along a half circle), the buffer layer was spin-coated over the uncovered core, and then an Au film was sputtered on it. The multilayer on the D-shaped POF contained a 60 nm thin Au film and a buffer layer with a thickness of 1.5 μm. The POF had a 980 μm core (polymethyl methacrylate) and 10 μm cladding (fluorinated polymer) in size. The SPR-POF sensor, a spectrometer (350 nm to 1023 nm), and a halogen lamp (360 nm to 1700 nm) coupled to a PC formed the basis of this straightforward and inexpensive experimental setup (Fig. 8). The process entailed building a unique MIP with binding sites engineered to identify perfluorinated chemicals (PFCs) precisely. A plasmonic POF, a type of optical fiber intended to facilitate the SPR processes, was combined with this MIP. The refractive index at the POF surface varied due to MIP interaction with PFCs. The exceptional capacity of the plasmonic POF to facilitate SPR makes the plasmonic component very important. The local refractive index near the point of foci changes as PFCs bind to the MIP, which causes noticeable changes in the SPR signal. Thus, PFCs can be directly and label-free detected in water samples employing our real-time SPR change monitoring technique.
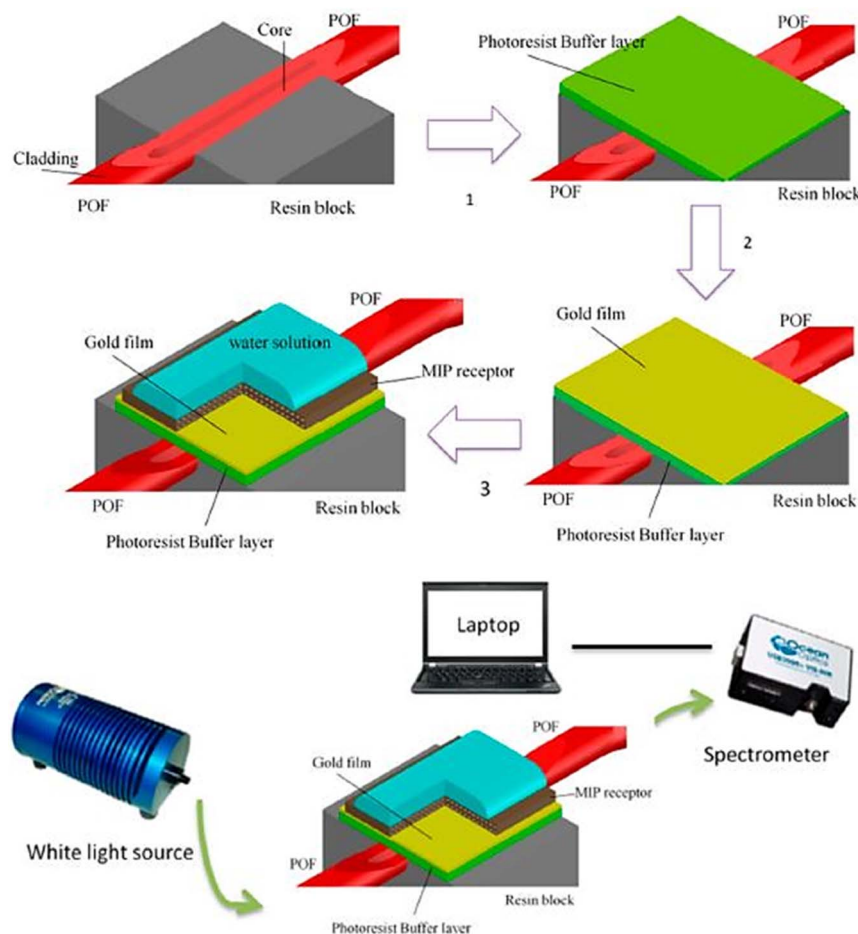

Fig. 8 Experimental setup and production techniques for implementing an SPR sensor in a D-shaped POF with an MIP receptor. Reproduced from ref. 89 Copyright 2018, MDBI.

Table 3 Comparison of various optical PFAS nano-sensors

Optical PFAS nano-sensor type	Detection principle	Sensitivity	Specificity	Real-time monitoring	Advantages	Disadvantages
Colorimetry	Color change in the presence of PFAS	Moderate	Limited	No (visual inspection)	Simple visual detection. No need for complex instrumentation	Limited sensitivity. Quantification may be challenging. Rapid response time
Fluorescence	Fluorescence quenching or enhancement in the presence of PFAS	High	High	Yes	High sensitivity. Quantitative analysis capability. Real-time monitoring	Susceptible to background fluorescence. Photobleaching may occur. Signal interference from the sample matrix
Optical scattering	Enhancement of Raman signals in the presence of PFAS	High	Molecular specificity	Yes	High sensitivity. Multiplexing capability. Molecular specificity	Signal reproducibility challenges. Complex fabrication processes
Plasmonic	Change in SPR signals upon binding of PFAS	High	High	Yes	Label-free sensing. Instantaneous monitoring. Highly sensitive	Equipment complexity and cost. Limited to thin sensing layers on the sensor surface

The label-free detection and real-time monitoring capabilities of SPR make it an advantageous tool for the detection of PFAS. Nevertheless, there are obstacles to overcome, such as the requirement for specialized tools and possible interference from intricate sample matrices. SPR-based biosensors for the detection of PFAS are being actively investigated by researchers, which is advancing environmental monitoring. Table 3 presents a comparative summary of the salient features of each type of optical PFAS nano-sensor, emphasizing their real-time monitoring capabilities, sensitivity, specificity, detection principles, benefits, and drawbacks.

5.2. Electrochemical PFAS nano-sensors

By applying the principles of electrochemistry to transform the binding events between PFAS molecules and sensing surfaces into detectable electrical signals, electrochemical nano-sensors present a viable approach for the detection PFAS.[90–92] Electrochemical sensors work based on the electrical current generated by oxidation–reduction reactions on the surface of electrodes.[93,94] Specifically, a conductive electrode surface is grafted with a selective chemical receptor, which is usually nanosized for improved sensitization and interacts with a target analyte.[95] This is the standard construction of an electrochemical sensor. A reference electrode, a counter electrode, and a functional anode or cathode electrode are the three electrode types often utilized in the system. The presence and quantity of the analyte are ascertained by comparing the variation in electric current across the electrode caused by the analyte molecule attaching to the receptor to calibration curves.

This technique often involves the use of different electrode materials and surface changes to improve the sensitivity and selectivity. As a result, it offers a reliable and effective way to monitor PFAS contamination in various environmental matrices.[96] There are many different types of electrochemical sensors, which are divided into different categories based on how strong an electrical signal they can detect. For instance, conductometric sensors measure changes in conductance (G), impedimetric sensors measure variations in impedance (Z) over a frequency (Hz) range, potentiometric sensors quantify variations in the ion-selective membrane potential (mV), and voltammetric sensors quantify the variation in current (pA) that results from the initial electrochemical reaction triggered by an applied voltage (mV). The two types of PFAS electrochemical sensors that are most often described are voltammetric and potentiometric. Table 4 represents the attributes of the reported electrochemical PFAS sensors.

5.2.1. Voltammetric PFAS nano-sensors. Voltammetric PFAS nano-sensors can precisely detect and measure PFAS chemicals using the electrical responses produced by voltammetric processes.[106] Enhancing the sensitivity and enabling real-time monitoring through integrating nanomaterials and advanced electrode modification methods meet the pressing requirement for effective PFAS detection in various environmental conditions such as pH fluctuation, salinity, and temperature. Pristine glassy carbon electrodes (GCE) were modified using a drop-casting method to add an ultrathin coating of gold nanostars (AuNS).[107] This modification aimed to increase the sensitivity of the electrode to ferrocene carboxylic acid, an electrochemical probe.[107] Subsequently, these AuNS-coated GCEs were further modified by adding a layer of o-phenylenediamine (o-PD) imprinted with perfluorooctanesulfonate (PFOS) using cyclic voltammetry for electropolymerization. This increased the sensitivity of the sensor to PFOS, as seen in Fig. 9A. Differential pulse voltammetry (DPV) was utilized to track the oxidation peak of ferrocene carboxylic acid (FcCOOH) in its Fe^{2+}/Fe^{3+} states to examine the dynamics of the interaction between the molecularly imprinted polymer (MIP) layer and

Table 4 Attributes of the reported electrochemical (EC) PFAS nano-sensors

EC sensor type	Platform nanomaterial	Receptor/probe	Target analyte	Mechanism/PFAS interaction	Range ($\mu g\ L^{-1}$)	LOD ($\mu g\ L^{-1}$)	Ref.
Voltammetry	Pt nanoelectrodes	Hydrogen gas	PFOA, PFOS	Hydrogen evolution reaction	$10–10^4$	30 (PFOA); 80 (PFOS)	97
	Au NPs	MIP of polydopamine	PFOS	—	0.01–8	0.0042	98
	B,N-Co-doped carbon nanowalls	MIP of poly(o-phenylenediamine)	PFOS	Carbon nanostructures create a distinctive arrangement of binding sites within MIPs, exhibiting a strong attraction to PFOS.	1×10^{-5}–5×10^{-2}	1.2	99
Potentiometry	Glassy carbon macro electrodes (radius 0.0015 m)	A thin layer (75 nm) of o-PD MIP	PFOS	When o-PD was anodically deposited in PFOS presence, it successfully prevented any heterogeneous electron transfer from occurring at the electrode and created MIPs	0–0.25	0.25	100
Photo-electrochemical	AgI nanoparticles–BiOI nanoflake arrays	MIPs of acrylamide	PFOA	The addition of PFOA results in a signal-off indirect photo-electrochemical process by increasing steric hindrance e^- transfer, and decreasing photocurrent	0.020–1000	0.1	101
	TiO$_2$ nanotube arrays	MIPs of polyacrylamide	PFOS	Increasing the concentration of PFOS proportionately increases photocurrent	250.06–50 012.60	86	102
	Screen-printed carbon electrodes modified with BiOI nanoflake arrays	MIPs of polyacrylamide	PFOSF	Adding PFOA results in a signal-off indirect photo-electrochemical process by increasing steric hindrance e^- transfer and decreasing photocurrent	0.05–500.00	0.01	103
Impedance	Interdigitated microelectrodes microfluidic probe	MOF Cr-MIL-101	PFOA	The unique shape of the MOF facilitates the convective transport of PFOS, leading to shorter diffusion times and the elimination of capacitance by the double layer	—	0.005	104
	B, N-co-doped carbon nanowalls	MIP of poly(o-phenylenediamine)	PFOS	Carbon nanostructures produce a unique array of binding sites within MIPs, demonstrating a pronounced affinity for PFOS.	1×10^{-5}–5×10^{-2}	1.2	99
Electrochemiluminescence	Ultrathin g-C$_3$N$_4$ nanosheets	MIPs of polypyrrole	PFOA	C–F bonding occurs, with a typical peak of F 1s at 688.8 eV & electrochemiluminescence signal "off"	50–400	20	105

8260 | J. Mater. Chem. A, 2025, 13, 8246–8281

This journal is © The Royal Society of Chemistry 2025

PFOS. The oxidation peak for the MIP/AuNS/GCE combination completely disappeared, as shown in Fig. 9A, before PFOS was removed, demonstrating the capacity of the MIP layer to prevent charge transfer between the working electrode and the solution. This voltammetric sensor shows promise in the detection of PFOS, with a 3σ method-calculated exceptionally low LOD of 0.015 nM. The proposed sensing probe demonstrated competence in identifying PFOS traces in tap water. Significant interferences were found during the experiments, especially with perfluorobutanoic acid (PFBA) or perfluorobutanesulfonic acid (PFBS). The smaller sizes of PFBA and PFBS molecules are

thought to be responsible for this interference phenomenon given that they allow them to get through the MIP layer and occupy PFOS-shaped voids through non-specific binding. Therefore, it is essential to perform a preliminary screening of unidentified samples to determine whether smaller PFAS molecules, including PFBA and PFBS, are present.

Electropolymerized molecularly imprinted poly(o-phenylenediamine) (o-PD MIPs) with a thickness of 170 ± 10 nm ($N = 3$) in combination with ferrocene carboxylic acid (FcCOOH) as a reversible redox probe was used to functionalize Au electrodes to counteract the low EC activity of PFOS, which is evident in the
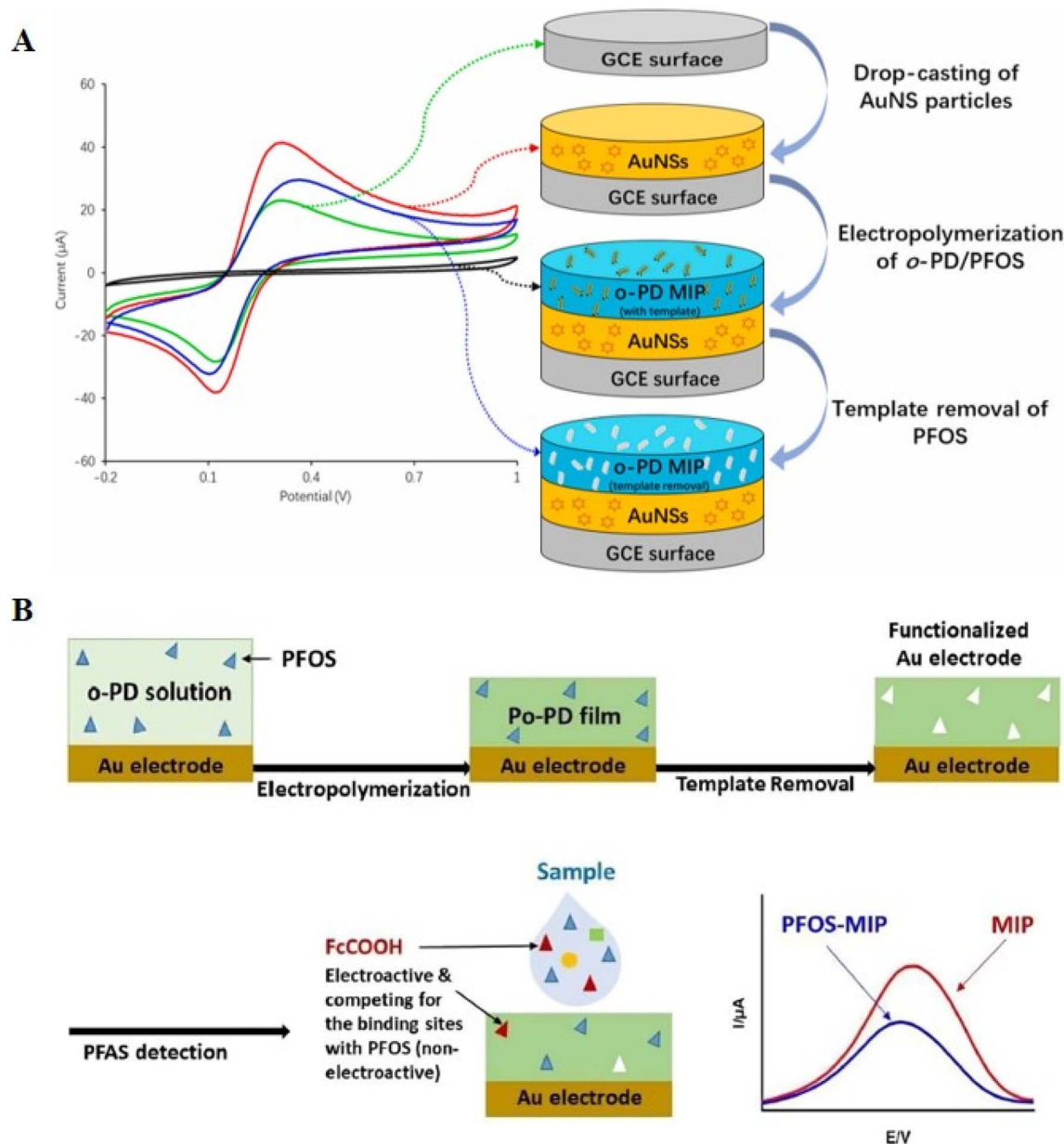

Fig. 9 (A) Representation of an improved voltammetric sensor for PFOS using gold nanostars (AuNS) and molecularly imprinted polymer (MIP). Reproduced from ref. 107 Copyright 2022, Elsevier. (B) Schematic of functionalized Au electrodes using electropolymerized and molecularly imprinted poly(o-phenylenediamine) (o-PD MIPs) in conjunction with ferrocene carboxylic acid (FcCOOH) as a reversible redox probe for voltammetric detection of PFOS. Reproduced from ref. 108 Copyright 2018, the American Chemical Society.

This journal is © The Royal Society of Chemistry 2025

J. Mater. Chem. A, 2025, **13**, 8246–8281 | **8261**

recorded voltammograms (Fig. 9B).[108] An LOD of 0.02 µg L^{-1} was obtained using two linear working ranges of 0.05–2.45 and 4.75–750.19 µg L^{-1}. This produced an LOD 10 times more sensitive than the ambient PL for PFOS at 0.2 µg L^{-1}. The voltammetric signal decreased when PFOS was present in the sample, establishing a correlation between the signal and PFOS content. The relationship between the concentration of PFOS in the solution and the voltammetric signal of the reporter molecule FcCOOH was shown to be inversely proportional.

One of the most important benefits of using voltammetric PFAS nano-sensors is that they can identify PFAS chemicals even at low concentrations, which makes it easier to respond quickly to environmental contamination incidents.[107] Additionally, adding nanomaterials improves the sensor performance by increasing the PFAS detection sensitivity and selectivity, as discussed above. However, certain issues still exist and require ongoing improvement. To facilitate the wide use of nano-sensors and regular monitoring, the high expenses related to their creation and operation must be addressed. Furthermore, improving the electron transfer conditions and addressing non-specific binding problems, mainly when interacting compounds are present, will improve the precision and dependability of PFAS nano-sensors in complex environmental samples. Voltammetric PFAS nano-sensors can confirm their position as indispensable instruments in the continuous endeavors to observe and lessen the effects of PFAS pollution on the environment by addressing these areas for development.

5.2.2. Potentiometric PFAS nano-sensors. Potentiometry, a method for measuring the voltage or electrical potential difference of a system, is the foundation on which potentiometric PFAS nano-sensors are based. The excellent sensitivity and selectivity of these nano-sensors are particularly engineered to detect PFAS. The interaction of PFAS compounds with the detecting components causes these nano-sensors to respond potentiometrically, as measured by electrical potential changes. This creative method uses nanotechnology to improve the PFAS detection accuracy, a breakthrough in environmental sensing.[109]

The electric potential drop by GenX PFAS binding to *o*-phenylenediamine (*o*-PD MIP) was examined. In this study, a significant blockage in the current flow was observed.[110] This strategy worked well for hexafluoropropylene oxide-dimer acid (HFPO-DA), a GenX PFAS, with an LOD of 0.000083 µg L^{-1}. Interestingly, this LOD was higher than LC-MS/MS sensitivity
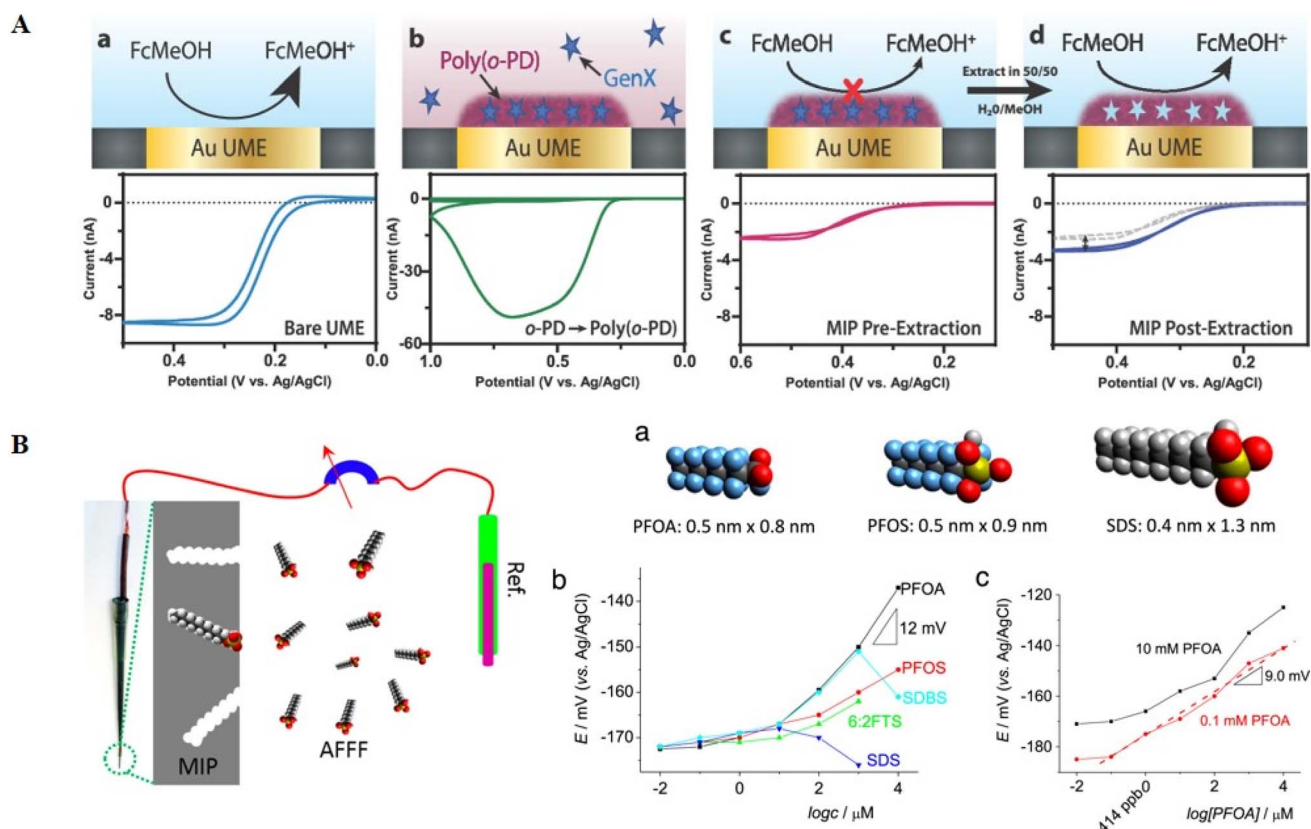

Fig. 10 A) Fabrication and functioning of µ-MIP: molecularly imprinted polymer–modified microelectrodes for the ultrasensitive quantification of GenX (HFPO-DA) by potentiometry: (a) oxidation of ferrocene methanol, producing a voltammogram and (b) electropolymerization of *o*-phenylenediamine, forming a molecularly imprinted polymer (MIP) that traps GenX molecules. (c) MIP layer insulating the electrode, affecting the current response during ferrocene methanol oxidation. (d) Extracting GenX exposes specific surface sites, influencing the current response, and in contaminated systems, GenX adsorption blocks surface sites correlating with analyte concentration. Reproduced from ref. 110 Copyright 2020, the American Chemical Society. (B) Schematic of the potentiometric response of PFOA-MIP depending on the concentrations of various anions and PFOA conditioning solution before the test. Reproduced from ref. 109 Copyright 2016, Elsevier.

8262 | *J. Mater. Chem. A*, 2025, **13**, 8246–8281

This journal is © The Royal Society of Chemistry 2025

$(0.0001\ \mu g\ L^{-1})$. This method involved coating a glassy carbon electrode with a 75 nm-thick layer of o-PD MIP using FcCOOH as a buffer (Fig. 10A). The inhibitory effect of the intercalation of PFOS with the MIP, which was connected to the PFOS content in the sample, resulted in a discernible loss in potential. Examining PFOS allowed the identification of concentrations as low as $0.025\ \mu g\ L^{-1}$, demonstrating a relative standard deviation of 6.2%. Notably, this sensitivity was 250-times lower than that of the LC-MS/MS technique. This method remained significantly more efficient, surpassing the PL of $0.2\ \mu g\ L^{-1}$ for PFOS and $0.4\ \mu g\ L^{-1}$ for PFOA by 8 and 16 times, respectively.[100]

A new method was applied to improve the development and production of potentiometric PFAS nano-sensors.[109] To accomplish the potentiometric detection of PFOA, an MIP was developed by electrodepositing polypyrrole (Py) with a thickness of ~600 nm onto a cheap electrode surface, specifically pencil lead (Fig. 10B). To improve the selectivity, methylene blue (MB) was added to the pyrrole polymer matrix. This was to promote the selectivity by facilitating ion pair formation involving fluoro-surfactants, often found in MB and aqueous film-forming foams (AFFFs). Consequently, this nano-sensor exhibited notable fluoro-surfactant detection capabilities, including PFOA, PFOS, and $1H,1H,2H,2H$-perfluorooctanesulfonic acid (6 : 2FTS), at concentrations in the range of 10 μM to 10 mM. The LOD for PFOA was notably reduced to around 100 nM, or 41 ppb, demonstrating the sensitivity and usefulness of this potentiometric nano-sensor in accurately and selectively identifying PFAS chemicals.

Potentiometric PFAS nano-sensors are useful tools for analytical and environmental applications because of their low detection limits and capacity for real-time monitoring. However, certain aspects still require further work to increase their overall performance, including managing the possible influence from intricate sample matrices, maintaining long-term stability, and maximizing scalability for broad use. Potentiometric PFAS nano-sensors have great promise, and thus further research and development efforts should be directed toward addressing these obstacles to facilitate their broader application in regulatory compliance and environmental monitoring.

5.2.3. **Photo-electrochemical PFAS nano-sensors.** Novel photo-electrochemical sensors (PEC sensors) based on photo-electric chemistry principles are emerging in the field of sensing technology.[111] These sensors are intended for the precise sensing of biological and chemical constituents. When exposed to light, the essential premise of PEC sensors is the creation of an electric current *via* the transfer of valence electrons inside the photoexcited material, which initiates chemical processes.[112] PEC sensors significantly limit the background noise by using light as the excitation source and photocurrents as recognition signals, resulting in increased sensitivity compared to traditional technology.[113] This novel technology takes advantage of the distinctive characteristics of light and photo-induced currents, establishing PEC sensors as viable instruments for improving the accuracy and sensitivity of molecular research.

A nanostructured probe for PEC sensing was constructed using MIP-modified AgI nanoparticle-BiOI nanoflake arrays as the photoactive electrode (designated as MIP@AgI-BiOINFs).[101] The MIP formation process is shown in Fig. 11A. The AgI-BiOINFs were produced *in situ* utilizing a simple sequential ionic layer adsorption and reaction (SILAR) method, which also served as the matrix for grafting the MIP recognition element. This PEC sensor detected PFOA with remarkable sensitivity and selectivity. In the absence of PFOA, triethanolamine (TEA) serves as an electron donor, amplifying the photocurrent on the modified electrode MIP@AgI-BiOINFs/FTO (where FTO refers to fluorine-doped tin oxide glass). Conversely, PFOA inhibits quencher molecules (TEA) from accessing the electrode surface and capturing photo-generated holes, impeding this process (Fig. 11B). The photocurrent gradually decreases until it ceases due to the steric barrier between AgI and PFOA caused by the adsorption of PFOA on the MIP@AgI-BiOINF arrays. The PEC analysis exhibited remarkable linearity in the PFOA concentration range of 0.02 to 1000.0 ppb, with an LOD of 0.01 ppb.

PEC sensors are inherently small, which makes it possible for them to be easily integrated into handheld devices, an essential feature for monitoring.[111] Their facile integration across various analytical domains, ranging from environmental monitoring to biological diagnostics, demonstrates their adaptability and promotes interdisciplinary applications. However, selecting ideal photoactive materials is crucial to the performance of PEC sensors, which makes customizing sensors for a given application difficult. Moreover, PEC sensors may be less accessible because of the complexity of the instrumentation needed for their deployment. Also, the considerable expenses linked to developing and implementing PEC sensor technology may impede its wider use. Thus, to address these challenges, research is being conducted, opening the door to the continuous development and use of photo-electrochemical sensors in various areas.[114,115]

5.2.4. **Impedance PFAS nano-sensors.** Impedance PFAS nano-sensors operate based on the principle of electrical impedance, measuring the opposition that PFAS compounds pose to the flow of an alternating current.[91] These nano-sensors leverage the interaction between PFAS molecules and a transducer surface, causing changes in the electrical impedance, which can be quantified. The impedance response is a sensitive and selective indicator, allowing the detection and estimation of PFAS in various environmental samples. This principle offers a foundation for designing advanced sensing technologies capable of addressing the challenges associated with PFAS monitoring and contributing to ecological safety.

The use of Au electrodes with o-PD MIPs for impedimetric measurements was more efficient than DPV.[116] With a sensitivity of $0.0001\ \mu g\ L^{-1}$, comparatively, the LC-MS/MS technique performed worse than this approach, demonstrating an LOD of $0.041\ \mu g\ L^{-1}$ for PFOA. Also, other researchers detected PFOS with an LOD of $0.00000102\ \mu g\ L^{-1}$ using Cu electrodes and polyester paper containing poly(aniline) MIPs (PANI).[117] According to an additional study, impedance PFAS nano-sensors have significant benefits. They can perform affinity-based capture operations with significant surface areas and
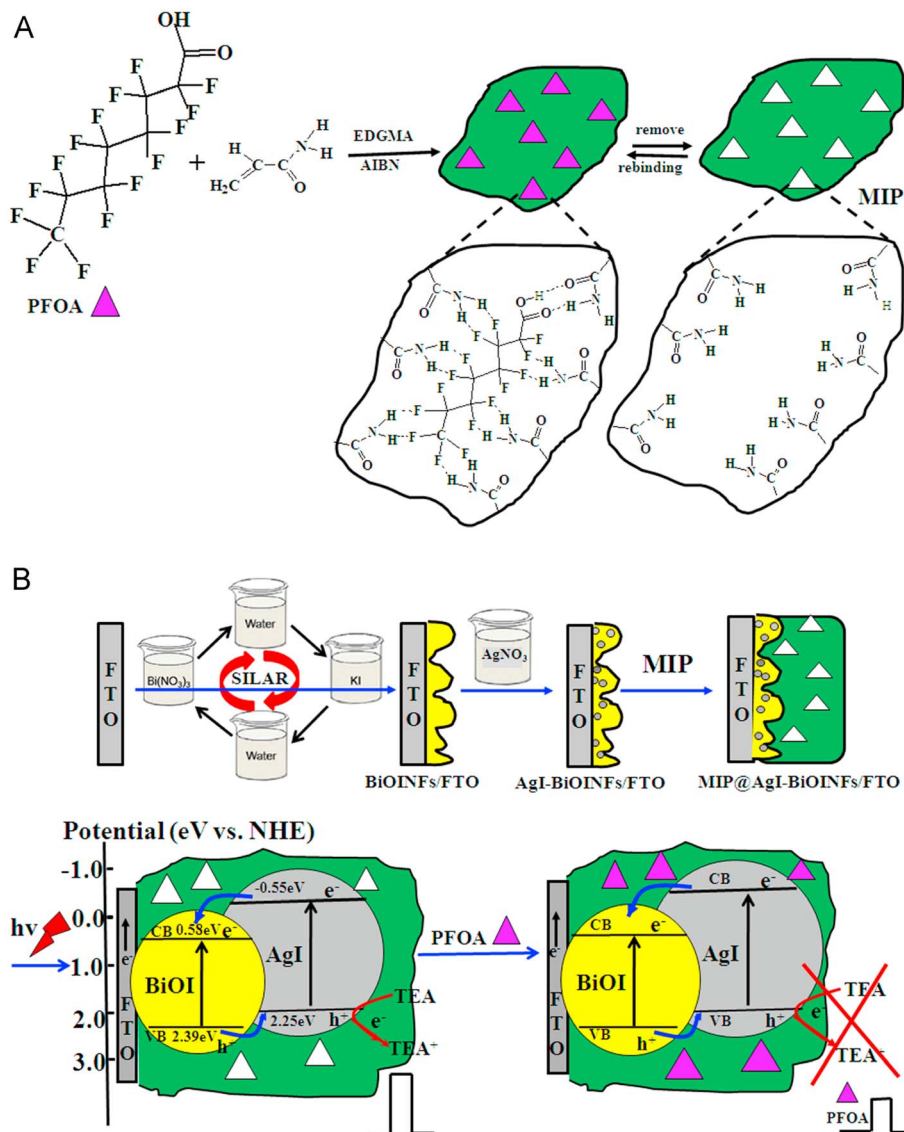
This journal is © The Royal Society of Chemistry 2025

J. Mater. Chem. A, 2025, **13**, 8246–8281 | **8263**

Fig. 11 A) Schematic of molecularly imprinted polymer (MIP) formation. (B) Schematic of the SILAR deposition of AgI–BiOINF films on MIP and the principle of PFOA PEC determination utilizing MIP@AgI-BiOINFs/FTO. Reproduced from ref. 101 Copyright 2015, Elsevier.

pore volumes, improving the detection capabilities with an LOD of 0.5 ng L^{-1}.[104]

The porous structure of MOFs combined with their enormous surface area (10^3–10^4 m^2 g^{-1}) enhances the number of interfaces and active sites suitable for interactions with specific compounds. Fig. 12A illustrates the range of contact modalities that MOFs and PFAS species display, including redox, electrostatic, H-bonding, hydrophobic, and attractive intermolecular fluorine–fluorine (F–F) interactions.[118,119] The precise composition of PFAS molecules and structural arrangement of MOFs determine the specific interactions occurring. Specifically, both quantum-chemistry simulations and empirical research show that the negatively charged fluorine functions in individual molecules are attracted to each another. They strategically integrated metal–organic frameworks (MOFs) such as Cr-MIL-101 into interdigitated microelectrodes (IDµEs) to enable

rapid detection, shorter reaction times, and the removal of reference electrodes (Fig. 12B). Furthermore, by using hydrogen bonds and electrostatic interactions, these nano-sensors showed an impressive performance for the identification of PFAS. The small number of publications emphasizes the early stages of this field of study, despite these developments. Thus, more research is needed, especially in verified reference colorimetric techniques, sensitivity, selectivity, and stability enhancements.

5.2.5. Electrochemiluminescence PFAS nano-sensors. Electrochemical processes and luminescence are combined in electrochemiluminescence (ECL) photofluorescence-based sensors to produce light.[120] These sensors are based on ECL-based sensing devices, which use high-energy electron processes to enable light emissions from luminophores. They serve as the foundation for the sensitive and targeted detection

8264 | J. Mater. Chem. A, 2025, **13**, 8246–8281

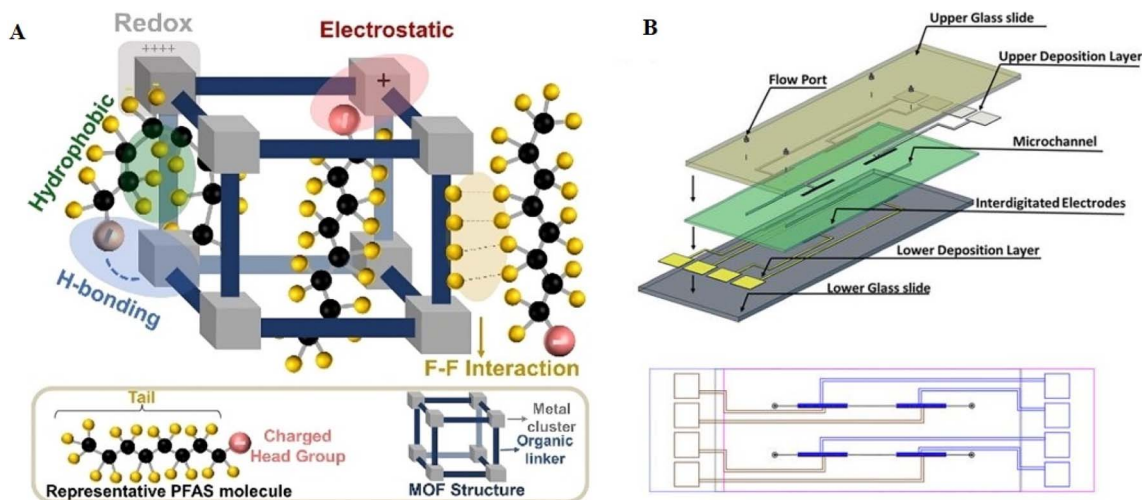This journal is © The Royal Society of Chemistry 2025

Fig. 12 (A) Depiction of the diverse interactions involving fluorinated MOFs and PFAS molecules, encompassing redox, electrostatic, hydrophobic, hydrogen bonding, and F–F interactions. Reproduced from ref. 118 Copyright 2022, John Wiley and Sons. (B) Illustration of the non-planar interdigitated device, showcasing a microchannel formed by a tape-cut and filled with Cr-MIL101. The microchannel is positioned between the upper and lower interdigitated microelectrode arrays, providing a top-view perspective). Reproduced from ref. 104 Copyright 2020, the American Chemical Society.

of PFAS.[121] These nano-sensors are usually comprised of nano-enhanced catalytic processes for PFAS breakdown, revealing the possibility of sustainable chemistry in converting PFAS compounds.[122] Furthermore, the advancement and use of innovative nano-sensor technologies are critical for the identification, tracking, and degradation of PFAS pollutants, with an emphasis on creative solutions for the detection of PFAS contamination at low levels in water sources. Carbon dots can contribute to the electrochemiluminescence sensing process, opening up new possibilities for PFAS detection.[123,124]

A novel electrochemiluminescence (ECL) sensor was constructed to detect PFOA. Using $S_2O_8^{2-}$ as a co-reactant, this sensor used 2D ultrathin $g\text{-}C_3N_4$ (utg-C_3N_4) nanosheets modified by molecularly imprinting polypyrrole as a cathodic ECL emitter (Fig. 13).[105] The utg-C_3N_4 nanosheets functionalized with MIP (MIP@utg-C_3N_4) exhibited an ECL signal with a consistent and notable enhancement. The ECL signal decreased due to the effective oxidation of the PFOA target by the electro-generated strong oxidant, namely $SO_4^{\cdot-}$ radicals produced by the reduction of the co-reactant $S_2O_8^{2-}$. This was attributed to the lower yield of excited utg-C_3N_4 (g-$C_3N_4^*$). This novel approach led to the development of a highly selective and sensitive MIP@utg-C_3N_4-based signal-off ECL sensor for the detection of PFOA. The newly developed ECL sensor demonstrated a linear response in two different PFOA concentration ranges of 0.02 to 40.0 ng mL^{-1} and 50.0–400.0 ng mL^{-1}. The estimated detection limit (S/N = 3) was 0.01 ng mL^{-1} (*i.e.*, 0.01 ppb), which is noteworthy given that it is comparable to the results from well-established LC-MS/MS techniques. However, electrochemiluminescent PFAS nano-sensors are still in the early stage of research. Thus, their further exploration and optimization are necessary for practical applications. Table 5 shows a brief comparison of various electrochemical PFAS nano-sensors.
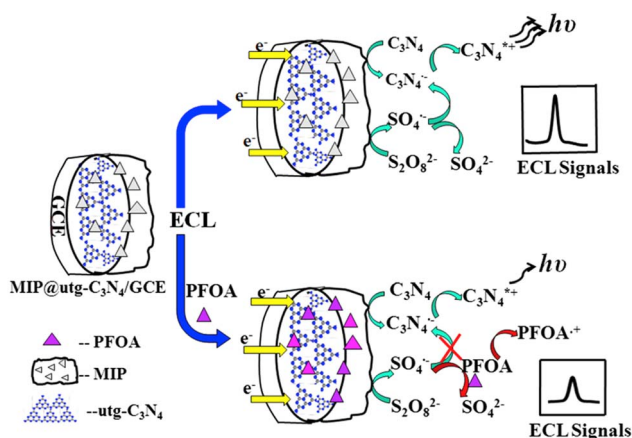

Fig. 13 Illustrative electrochemiluminescence detection technique for PFOA with MIP-functionalized utg-C_3N_4 in $S_2O_8^{2-}$ system. Reproduced from ref. 105 Copyright 2015, Elsevier.

5.3. Aptamer-based PFAS nano-sensors

Aptamer-based PFAS nano-sensors provide a very sensitive and selective method for detecting PFAS. These nano-sensors take advantage of the unique capabilities of aptamers, single-stranded DNA, or RNA, which can attach to particular molecules of interest.[125,126] The basic idea is to create aptamers with selectivity for PFAS, allowing the development of nanoscale sensors capable of detecting and measuring these pollutants in water and other environmental samples.[127] SELEX, which stands for sequential evolution of ligands by exponential enrichment, is a technique that selects aptamers with affinity for a specific target from a huge oligonucleotide library. The SELEX procedure generates 10^6 aptamer sequences. At the base pair level, finding the best candidates is a sophisticated process that uses various analytical tools. The engineered aptamer can interact with the target with different binding mechanisms such

This journal is © The Royal Society of Chemistry 2025

J. Mater. Chem. A, 2025, **13**, 8246–8281 | **8265**

Table 5 Comparison of various electrochemical PFAS nano-sensors

Electrochemical PFAS nano-sensor type	Detection principle	Sensitivity	Specificity	Real-time monitoring	Advantages	Disadvantages
Voltammetry	Electrochemical redox reactions	High	Moderate	Limited	High sensitivity, simple operation	Limited specificity may require complex electrodes
Potentiometry	Potential difference measurement	Moderate	High	Limited	High specificity, stable signal	Slower response compared to some techniques
Photo-electrochemical	Light-induced redox reactions	Moderate to high	High	Limited	Selective and sensitive, potential for miniaturization	Complex instrumentation, sensitivity to light conditions
Impedance	Measurement of electrical impedance	Moderate to high	Moderate to high	Possible	Label-free, potential for real-time monitoring	Limited feature prominence at higher frequencies
Electrochemiluminescence	Electrochemical process producing light	High	High	Possible	High sensitivity, low detection limits	Instrumentation complexity, limited to specific PFAS

Fig. 14 (A) Schematic of the structure and mechanisms of aptamer target complex formation. Reproduced from ref. 128 Copyright 2013, Swiss Med Wkly. (B) PFOA_JYP_2 predicted 2D structures with 0 mM PFOA & 0.5 mM PFOA and 1D-^{1}H NMR spectra showing the changes in Watson–Crick pairing and non-canonical pairing before and after adding & 0.5 mM PFO. Reproduced from ref. 129 Copyright 2022, Elsevier.

as induced fit, structural compatibility, electrostatic interaction, and hydrogen bridges (Fig. 14A).[128]

Environmental sensing has advanced significantly since the use of DNA aptamers was pioneered to detect PFAS and related fluorinated chemicals.[129] Owing to its unique binding affinity to PFOA, a designed aptamer was easily integrated into a fluorescence-based aptamer sensor, allowing the sensing of aqueous PFOA at a remarkable LOD of 0.17 μM. The conformational shift

8266 | *J. Mater. Chem. A*, 2025, **13**, 8246–8281

This journal is © The Royal Society of Chemistry 2025

in the aptamer upon interaction with PFOA mitigated the quenching impact on the fluorescence of fluorescein, which was the basis for the sensing mechanism. Structural insights are displayed in Fig. 14B, indicating the expected configuration of the 30-base aptamer after binding PFOA. The aptamer was combined with PFOA solutions at varying concentrations (0.5–50 μM) for the experimental evaluation. The fluorescence intensity was measured after 40 min of incubation, showing a linear increase with increasing PFOA concentrations.

Using 1D-^{1}H and 2D NOESY NMR methods, the secondary structure of the PFOA_JYP_2 aptamer was investigated both with and without PFOA (Fig. 14B).[129] Changes in the chemical shifts in the range of 10–14 ppm were seen in 1D-^{1}H NMR spectra, corresponding to the imino protons of the guanine (G) and thymine (T) bases.[130] In the absence of PFOA, the aptamer displayed two peaks at 13.4 and 13.5 ppm and five peaks at 12.4,

12.44, 12.5, 12.6, and 12.8 ppm, signifying two thymines and five guanines, respectively, in the Watson–Crick base pairing range (12–14 ppm). New peaks appeared at 12.1, 12.2, 12.7, and 13.6 ppm in the presence of PFOA, indicating three guanines and one thymine. Furthermore, peaks (e.g., 10.5, 10.8, 11.3, 11.5, and 11.8 ppm) that correspond to non-Watson–Crick base guanines and thymines emerged in the range of 10–12 ppm. According to Neves and colleagues, the appearance of these base pairs indicated conformational alterations and aptamer folding caused by contact with PFOA.[131]

Significantly, the sensor demonstrated very low sensitivity to interferences, as demonstrated by its effective use in wastewater discharge monitoring.[129] The aptamer sensor based on fluorescence exhibited exceptional sensitivity, making it especially appropriate for detecting levels of PFOA in water close to unintentional spills and manufacturing regions where elevated
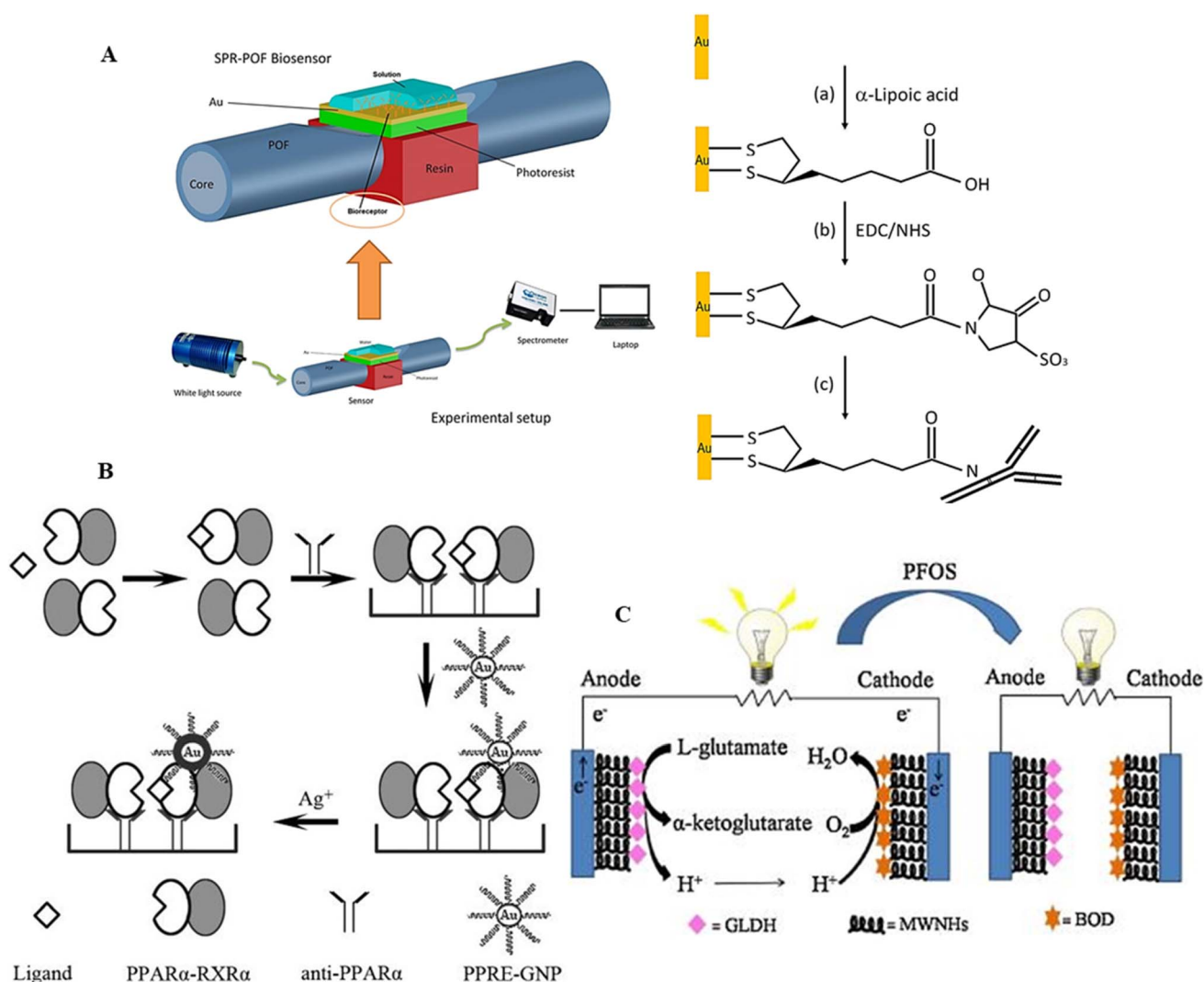

Fig. 15 (A) Schematic of optical immunosensor surface functionalized with gold system based on POF-SPR platform. Reproduced from ref. 134 Copyright 2018, Elsevier. (B) Schematic of PFOS detection based on the interaction between PPRE-modified gold nanoparticle probes and activated PPARα with silver. Reproduced from ref. 135 Copyright 2011, Elsevier. (C) Illustration of an electrochemical immunosensor for the highly sensitive detection of PFOS. This sensor utilizes glassy carbon electrodes (GCE) modified with multi-walled carbon nanohorns (MWNHs) as substrates for both bioanode and biocathode. Biocatalysts, namely glutamic dehydrogenase (GLDH) and bilirubin oxidase (BOD), are employed in the detection process. Reproduced from ref. 136 Copyright 2014, the Electrochemical Society of Japan.

This journal is © The Royal Society of Chemistry 2025

J. Mater. Chem. A, 2025, 13, 8246–8281 | 8267

amounts of PFAS are predictable. Although the present LOD cannot measure concentrations below regulatory limits, fluorescence-based sensors have an advantage in that they can function in solution without requiring immobilization of the receptor on solid supports. Thus far, this is the only report of PFAS detection using aptamers.

5.4. Immunonanosensors for PFAS

Immunonanosensors for the detection of PFAS using particular antibodies or antigens have been reported to gather and determine PFAS molecules. These nano-sensors exploit the extremely specific binding interactions of antibodies with PFAS chemicals, enabling sensitive and accurate detection. The immobilization of these identification components on nano-materials increases the sensor surface area, allowing a greater binding capacity and enhancing the overall PFAS detection performance.[132]

Monoclonal and custom-designed antibodies, often created through a surrogate for amplification, were employed to achieve precise and selective binding of PFA compounds.[133] Utilizing monoclonal antibodies targeting α-lipoic acid compounds, self-assembled monolayers of these antibodies were affixed onto the surface of plastic optical fibers (POF) by Cennamo and colleagues (Fig. 15A).[134] This immunonanosensor showed an LOD of 0.21 μg L^{-1} for both PFOS and PFOA. These sensors formed self-assembling monolayers on plastic optical fiber surfaces by grafting antibodies created using an enzyme-linked immunosorbent assay (ELISA) onto AuNPs functionalized with α-lipophilic acid molecules. SPR was used for signal detection, and MIPs were attached to AuNPs to act as a sensing platform. The recognition event, governed by the anionic functional groups of PFAS and van der Waals interactions, induced measurable signals and resonant wavelength shifts upon contact with PFOS/PFOA, reflecting changes in refractive index.[137]

As an agonist for peroxisome proliferator-activated receptor alpha (PPAR), PFAS has ramifications in activating several target genes *via* this transcription factor. A new immunona-nosensor captured the active PPAR complex using monoclonal anti-PPAR antibodies on a microplate.[135] In this system, AuNPs modified with PPARα-responsive elements (PPRE) selectively bind to the activated complex, and silver was introduced to amplify the signal, exhibiting a positive correlation with PFOS concentration and achieving a low detection limit of 5 ppt (Fig. 15B). Another sensor employed streptavidin-modified quantum dots (QDs) as a fluorescent marker that binds to the PFOS-activated PPARα complex.[138] The PFOS concentration was directly correlated with the fluorescence intensity of the QDs, with a low detection limit of 2.5 ppt. Although PPARα sensors are promising, their field adaptability is limited due to the repeated reagent addition, washing, and incubation processes they currently need. The application of this approach can be increased by converting it to the lateral flow assay format, allowing the on-site determination of total PFAS concentration.

Using modified glassy carbon electrodes (GCE) as the bio-anode and biocathode substrates and glutamic dehydrogenase (GLDH) and bilirubin oxidase (BOD) as biocatalysts, an inno-vative electrochemical immunosensor was developed for the sensitive detection of PFOS (Fig. 15C).[136] This immunosensor made use of the inhibitory effect of PFOS on biocatalysis within an enzymatic biofuel cell (BFC). The one-compartment BFC had an open circuit potential (V_{oc}) of 30.65 mV and maximum power density of 27.5 W cm^{-2}. The biosensor displayed a broad linear detection range of 5 to 500 nmol L^{-1} based on the V_{oc} and PFOS concentration. It also demonstrated a significant correlation ($R^2 = 0.976$) with a measurement frequency of three times ($n = 3$). The PFOS may further lower the open circuit voltage of the BFC by blocking the enzymatic activity of bilirubin oxidase and glutamic dehydrogenase. Following a 20 min interaction,

Table 6 Comparison of the nano-sensors for PFAS detection[a]

Type of sensor	LOD (ng L^{-1})	LOQ (ng L^{-1})	Sensitivity	Major advantages	Major disadvantages
Optical sensors	0.1–10	0.5–50	High; dependent on fluorophore or chromophore properties	High specificity and rapid detection; suitable for real-time monitoring; non-invasive methods	High cost of instrumentation; may require complex sample preparation for environmental matrices
Electrochemical sensors	1–100	5–200	High; depends on electrode material and surface modifications	Simple instrumentation; portable and cost-effective; amenable to on-site applications	May suffer from electrode fouling; requires precise calibration for environmental samples
Aptamer-based sensors	0.01–1	0.05–5	Very high; aptamers offer strong binding affinity and specificity	Highly specific recognition of PFAS; tunable for different PFAS compounds; reusable in certain formats	Production of aptamers can be costly and time-consuming; stability may be limited under environmental conditions
Immunosensors	0.1–5	0.5–20	High; depends on antibody–antigen interactions	High specificity; adaptable to multiple formats (*e.g.*, ELISA, lateral flow assays); well-established methods	Expensive antibodies; limited reusability; potential for cross-reactivity among structurally similar PFAS

[a] LOD* – limit of detection and LOQ** – limit of quantification.

8268 | *J. Mater. Chem. A*, 2025, **13**, 8246–8281

This journal is © The Royal Society of Chemistry 2025

the detection limit was 1.6 nmol L^{-1}. Furthermore, in micro-polluted water, the biosensor demonstrated significant selectivity for PFOS over structurally related perfluorinated compounds and contemporaneous molecules (SMNBS and SDS). For the PFOS detection in complex aqueous matrices using the standard addition technique, precision was confirmed with an RSD ranging from 3.6% to 7.7%. Table 6 presents a broader overview of the reported nano-sensors for the detection of PFAS.

6. Possible mechanism of interaction of PFAS with nano-probes

The implementation of different materials for the sensing or removal of PFAS has been challenging because the water stream to be decontaminated contains organic molecules with a concentration $2.5 \pm 0.3 \times 10^6$ times higher than the PFAS, and the remediation of the water source will lead to the concentration of the non-fluorinated organic molecules, whereas the

Fig. 16 Representation of different types of molecular-level interaction pertaining to sensing and remediation of PFAS molecules in aqueous solution. (A) Fluorophilic interaction (dashed lines) occurring between a fluorinated carbon substrate and PFOS. (B) Electrostatic interaction occurring between quaternary ammonium cation and the PFOS anion. (C) Ammonium cations that are part of an anion exchange resin, where the PFOS anion faces strong electrostatic interaction to separate from the aqueous elution phase. (D) Water present in the systems attaining its stable structure by phasing out the carbon material to participate in hydrophobic interaction with the carbon chain of PFOS. (E) Carboxylate-derived carbon support participating in sensing of PFOS anions *via* Ca^{2+} cation bridge interaction. (F) Carboxylic acid groups of the substrate and the PFAS interacting *via* hydrogen bonding interactions. (G) van der Waals interaction stabilizing solution-phase self-assembly of PFOS in aqueous solution. (H) $\pi-\pi$ interaction leading to adsorption of the phenyl substituted PFAS over carbon material having π-delocalized system.

This journal is © The Royal Society of Chemistry 2025

J. Mater. Chem. A, 2025, **13**, 8246–8281 | **8269**

majority of the PFAS will still be present in water bodies.[32] Polluted groundwater streams also contain different particles (micro to nano dimensional) and dissolved salts. The solution phase sorption of PFAS depends on the net free energy change accompanying the interactional transition of PFAS molecules from the aqueous phase to the solid phase. This can be a combination of both (i) solvation effects such as enthalpy and entropy changes associated with solvent–solvent, solute–solvent, and solvent–sorbent interaction and (ii) molecular interactions between the solute and sorbent. Thus, in this section, we highlight different chemical interactions as possible sources for the selective sensing and removal of PFAS from water bodies. Fig. 16 summarises all the possible interactions of the PFAS moiety with nano-probes.

6.1. Fluorophilic interactions

Non-bonding interactions are decisive in recognizing two or more molecular entities, which is crucial for sensing inert entities such as PFAS. The C–F bonds may participate in dipole–dipole and point dipole interaction with ionic groups and dipolar groups, which can lead to C–F···F–C intermolecular dispersion interactions, often referred to as fluorophilic interactions.[139] This fluorophilic interaction is weak, but its magnitude depends on the number of interacting groups (Fig. 16A). This proposition can be easily supported by literature reports, where ionic fluorogels and magnetic fluorinated polymers were employed for PFAS removal from water sources, which showed high affinity and high capacity of PFAS removal from water bodies compared to non-fluorinated versions of the sorbents.[23,140] The removal efficiencies drastically decreased with a decrease in the chain length of the PFAS, resulting in a decrease in the sorption properties of the fluorinated polymer. Thus, in sensing small-chain PFAS molecules, electrostatic interactions may play a governing role over fluorophilic interactions.[141]

6.2. Electrostatic interactions

Electrostatic interaction is a form of non-covalent interaction between charged particles that can be attractive as well as repulsive. There are two sources of electrostatic interaction in PFAS, the first being the low pK_a of PFAS in an aqueous solution.[142] Owing to the electron-withdrawing effect of the fluoroalkyl chains, the head group containing CO_2 and SO_3 is always in its ionic form (Fig. 16B). Long-chain PFAS are the most common in the aquatic environment. With concentrations above 1000 ppm, they can form micelles or hemimicelles in groundwater, attaining stability in the aquatic environment. PFAS can also aggregate with foreign particles suspended in water bodies to form aggregation even at concentrations lower than their CMC. PFAS are generally found as anions, but depending on the pH and functional groups present, they can be anionic, cationic, and zwitterionic.[143] In the case of anionic PFAS, when the solution pH is below the pK_a, they exist as neutral molecules, whereas above the pK_a value, as anions. This is the opposite in the case of cationic PFAS, where at lower pH values than pK_a they exist in the cationic form; otherwise, in the

neutral form. However, in the case of zwitterionic PFAS, when the solution pH is lower than the first pK_a, they exist as cations, and higher than the second pK_a, as anions. When the pH of the solution is between these two limiting values, PFAS exist as charge neutralized species with separate cationic and anionic functionalities. Thus, the sensing of cationic and zwitterionic PFAS is strongly dependent on the pH of the solution. This affects their transportation and adsorption, posing severe difficulties in the design of materials for the remediation of these species. Based on electrostatic interactions and hydrophobic interactions, the uptake of PFAS can be accomplished from water sources by ion exchangers.

6.3. Ion exchange

Ion exchange resin attracts molecules of opposite charge and releases an equal number of the same charged ions to an aqueous solution until equilibrium is established.[119] The effectiveness of this process depends on different factors including the charge on the PFAS ion, the charge density of the PFAS ions, the polarizability of the ions, the degree of cross-linking of the ion exchange resin, the ion exchange capacity of the resin, the functional groups present in the ion exchanger, and nature and concentration of the eluted ions.[43] Among them, the most crucial factor is the ion exchange capacity of the resin, which varies with the pH of the solution and may affect the uptake of PFAS with an increase in pH (Fig. 16C). Also, the coexistence of other anions in the solution may compete with the uptake of PFAS, making the presence of hydrophobic interaction a governing factor in the PFAS uptake.[144]

6.4. Hydrophobic interaction

Structurally, PFAS are comprised of a hydrophobic tail predominantly due to their C–F bonds and a hydrophilic head comprised of sulphonic acid and carboxylic acid head groups. This type of interaction describes the strong interaction between a hydrophobic molecule and a hydrophobic carbon surface.[145] One of the cheapest and benchmark materials for PFAS sensing is activated carbon, which is already used for remediation and filtering applications.[146] Electrostatic and non-electrostatic interactions drive the adsorption of molecules such as PFAS on activated carbon. In the case of non-electrostatic interactions, they include dispersion and hydrophobic interaction, whereas electrostatic or coulombic interaction applies for PFAS in dissociated form in aqueous condition. The adsorption of PFAS over activated carbon is a result of their surface composition and heteroatom content, mainly surface oxygen content. When a material such as activated carbon, carbon dots, or graphene is immersed in an aqueous solution, it either attains ionic form by dissociating its surface functionalities or absorbs the ion in the solution to develop a surface charge.[147] The negative surface charge originates from the dissociation of surface functionalities such as carboxylates, sulphonates, or phenolic groups. The positively charged character of the surface originates from the adsorption of positively charged metal ions on the surface and due to the electron density, acting as a Lewis base and abstracting protons from the

8270 | *J. Mater. Chem. A*, 2025, **13**, 8246–8281

This journal is © The Royal Society of Chemistry 2025

solution. Thus, the development of surface charge by carbon materials enhances the possibilities of electrostatic interaction with PAFS, leading to their adsorption. The surface oxygen content also dictates the hydrophobic interaction between the hydrophobic PFAS molecule and the hydrophobic carbon surface.[148] The water molecules in aqueous solution have a strong tendency to associate with each other to retain their structure, thus phasing out the hydrophobic components to form a separate phase (Fig. 16D). Therefore, hydrophobic interaction is advantageous for the sensing and remediation of long-chain PFAS molecules in the aqueous environment.

6.5. Cation bridge interaction

PFAS molecules, including long-chain PFSA and short-chain PFCA, showed enhanced sorption in the presence of divalent cationic species.[149] This was not only due to the pH of the solution but also an effect of the ionic strength in the charge neutralization of anionic PFAS. Finally, the formation of cationic bridges between the −ve-charged head group of the PFAS molecules and the −ve-charged surface of the absorber is under investigation. The effect is small for short-chain PFAS but stronger for the long-chain PFAS and becomes a predominant factor with an increase in the charge density of the cations in the solution. This phenomenon has excellent benefits when polyvalent cations are used, which helps better pack PFAS molecules on the adsorbent surface.[150] Generally, the adsorption of PFAS on surfaces decreases with an increase in pH. However, the opposite trend was observed due to the presence of divalent cations in the solution given that the alkalinity of the solution increased the −ve charge density of the absorbent surface, improving the cation bridge interaction (Fig. 16E). Besides this, the divalent cation can also bridge two PFAS anions in the solution. Single-atom functionalized graphene and carbon dots can be very effective in PFAS remediation given that the transition metal single atoms are supported or stabilized by primary, secondary, or tertiary amine-based donors or carboxylate functionalities and can favourably interact with anionic PFAS *via* salt bridge interaction, leading counterion ion condensation and phase separation.

6.6. Hydrogen bonding

The fluorocarbon tail of PFAS does not participate in H-bonding interaction due to the high stabilization of the s and p orbitals, making the F groups nonpolarizable and a poor acceptor of hydrogen bonds, but the oxygen atoms present in the head functional groups are suitable hydrogen bonding acceptors (Fig. 16F). PFAS show weak intermolecular interaction with the surrounding phase, which is the leading cause of their mobility and persistent air pollution unless strong forces such as hydrogen bonding interaction between the head group and the water molecules hold them together.[143] PFAS molecules in the ionized form at the air–water interface interact to form a belt of hydrogen bonding interactions.[151] This interaction may help PFAS in foam stabilization and decrease their mobility. pH influences the extent of H-bonding of the PFAS at the air–water interface, where the pK_a of PFAS at the surface and bulk is

different, leading to the formation of dissimilar aggregation states.[152] Aggregation can also be caused due to contributions from van der Waals interaction.

6.7. van der Waals interaction

Weak intermolecular interaction is the leading cause of micellization or aggregation of PFAS.[153] In the long-range interactions, the particles tend to attract each other due to van der Waals forces, and based on the contribution of other interacting forces such as electrostatic interaction, they come close to each other, whereas the van der Waals forces tend to repel each other. This particle–particle interaction with respect to separation distance causes the stabilization of colloidal PFAS solutions (Fig. 16G). This can be essential in sensing and separating PFAS in aqueous solution.

6.8. π–π interaction

In the case of PFAS having phenyl aromatic rings as substituents, they have a crucial driving force in the form of π–π interaction to get absorbed on the surface of absorbers having a π-electron cloud (Fig. 16H). Here, one of the systems with an electron-rich moiety containing a π-electron cloud acts as a donor, interacting with entities that have electron-deficient π-electron systems, leading to donor–acceptor π–π interaction.[154]

Based on the aforementioned molecular level interactions, metal single-atom-supported graphene and carbon dots (CDs) can be a viable substrate for sensing PFAS.[61,155,156] To support our proposition, here we highlight the role of graphene and carbon dot substrates in sensing applications. CDs possess excellent optical properties with strong absorption and emission properties with high photostability. CDs were implemented for sensing Hg^{2+} in tap water and mineral water. The surface functionalities of CDs such as carboxyl and ammine groups led to the enhanced optical sensing of Hg^{2+} with a sensitivity in the ppb range. The strong metal–CD support interaction not only perturbed the photoexcited state of the CDs but also decreased the lifetime of the Hg^{2+}-CD photoexcited state, which decreased with an increase in the concentration of the Hg^{2+} in the solution.[157] Thus, metal single-atom functionalized CDs can be a viable substrate for the optical sensing of PFAS owing to the strong electrostatic interaction between the positively charged single metal atom and negatively charged PFAS molecules and hydrophobic and strong van der Waals interaction between the CD substrate and the PFAS molecules. Different extents of interaction with different first–row transition metal atoms may also lead to the selective lifetime-based sensing of PFAS. Alternatively, functionalized graphene and its quantum dot interface have been well studied in the substitution of different functionalities, which have strong interaction with metal ions, leading to the formation of single-atom graphene materials.[158,159] By virtue of the high electron mobility facilitated by graphene, the selectivity of intermolecular interactions imparted by the surface functionalities and redox properties by transition metal single atoms, it becomes an excellent candidate for the electrochemical sensing of PFAS.[160] Substrates such as fluorographene may lead to enhanced

This journal is © The Royal Society of Chemistry 2025

J. Mater. Chem. A, 2025, **13**, 8246–8281 | 8271

fluorophilic interaction, hydrophobic interaction in the carbon framework, and the single metal sites in electrostatic interaction may lead to enhanced selectivity for PFAS sensing over the hydrocarbons present in water bodies.[147] The added benefit of graphene-based systems is that they can participate in π–π interaction with PFAS, leading to their selective detection with phenyl substituents over the saturated carbon-chained PFAS.

7. Techniques for PFAS removal and integration with electrochemical methods using nanomaterials

PFAS removal is a crucial task because of their chemical stability, persistence, and extensive environmental presence. Adsorption, advanced oxidation processes (AOPs), membrane filtering, and biological approaches are all common methods for the removal of PFAS, each having its own level of efficiency and limitations. Recent advances in nanomaterials have considerably improved the effectiveness of these treatments, particularly when combined with electrochemical methods, allowing more inventive and economical PFAS remediation.

7.1. Adsorption

Nanomaterials such as carbon nanotubes, graphene oxide, MOFs, and functionalized silica have high surface areas, tunable porosity, and functional surface groups, making them effective PFAS adsorbents.[161,162] For example, carbon dots functionalized with amines or quaternary ammonium groups interact strongly with PFAS via electrostatic and hydrophobic forces. Integrating these nanoparticles into adsorption columns or filters can result in excellent PFAS removal effectiveness, even at low concentrations.

7.2. Advanced oxidation processes

Advanced oxidation processes (AOPs) employ nanomaterials such as TiO_2 and doped ZnO nanoparticles to destroy PFAS using photocatalytic processes.[163] When triggered by UV or visible light, these nanoparticles produce reactive oxygen species (ROS), which can degrade PFAS into shorter-chain chemicals or mineralize them entirely. Doping TiO_2 with fluorine or nitrogen can enhance light absorption in the visible spectrum, leading to higher efficiency in real-world situations.

7.3. Membrane filtration

Nanomaterial-enabled membranes, including graphene oxide-coated or nanofiber membranes, improve classic filtering methods such as reverse osmosis (RO) and nanofiltration (NF).[164,165] The exact pore diameters and chemical selectivity of these membranes allow them to successfully reject PFAS compounds. Furthermore, they have antifouling qualities that increase their operating longevity.

7.4. Biological methods

Nanomaterials can promote microbial systems by functioning as electron carriers or catalytic sites, despite the resistance of PFAS to biodegradation.[166] Biochar and carbon nanotubes, for example, can aid in the breakdown of PFAS precursors by facilitating electron transfer during microbial degradation processes.

7.5. Integration of electrochemical techniques with nanomaterial-based approaches

Electrochemical approaches, such as electrochemical oxidation, reduction, and electrocatalysis, provide potential avenues for the degradation of PFAS.[167] These approaches can be successfully combined with nanomaterial-based PFAS removal strategies to overcome their individual limitations and improve their performance.

7.5.1. Electrochemical oxidation coupled with adsorption. Nanomaterials such as carbon nanotubes and MOFs can absorb and concentrate PFAS in water by electrochemical oxidation and adsorption. Subsequently, electrochemical oxidation can be employed to destroy the adsorbed PFAS on the adsorbent, renewing the nanomaterial for future usage. For example, when paired with carbon-based adsorbents, boron-doped diamond (BDD) electrodes may effectively oxidize PFAS, resulting in the near-complete mineralization of pollutants.

7.5.2. Electro-Fenton processes with nanomaterials. Electro-Fenton processes, which produce hydroxyl radicals through electrochemical reactions, can be enhanced using nanocatalysts such as iron oxide nanoparticles. These nanoparticles serve as either homogeneous or heterogeneous catalysts, boosting ROS generation and increasing the PFAS breakdown rates. Magnetic nanoparticles, for example, make it easier to recover and reuse materials, hence boosting the process sustainability.

7.5.3. Electrochemical membrane reactors. Nanomaterial-coated membranes, including graphene oxide and carbon nanotubes, can function as electrochemical reactors. Using an electric potential, these membranes can destroy PFAS molecules, while also purifying water. This dual functionality lowers energy usage and operational complexity.

In conclusion, combining electrochemical techniques with nanomaterial-based PFAS removal technologies provides a very effective and long-term solution to the issues faced by PFAS contamination. Nanomaterials such as carbon-based adsorbents, catalytic nanoparticles, and improved membranes improve the effectiveness of adsorption, AOPs, and filtering processes, while electrochemical approaches provide effective routes for PFAS degradation and material regeneration. By harnessing the synergies between these technologies, it is feasible to obtain better removal rates, lower energy usage, and less secondary waste. Continued study and development of these integrated systems will be essential for developing scalable and cost-effective PFAS remediation methods.

8. Challenges, prospects, and conclusion

Due to the ubiquitous and persistent character of per- and PFAS, the accurate sensing of these pollutants is critical for successful

8272 | *J. Mater. Chem. A*, 2025, **13**, 8246–8281

This journal is © The Royal Society of Chemistry 2025

environmental monitoring. PFAS are found in diverse matrices, including water, soil, and air, and pose a substantial hazard to the ecosystem and human health. Sensing technologies are critical in measuring PFAS concentrations in these samples, giving necessary data for risk assessment and informed decision-making. Real-time and accurate detection tools, such as sensors created particularly for PFAS, provide significant information on contamination. A dependable PFAS sensor can provide near-instant data capturing to allow rapid actions to limit exposure hazards. Furthermore, they present critical levels of data for water quality managers, government agencies, and communities for implementing targeted remediation plans and ensuring regulatory compliance.

The sensing of PFAS poses considerable hurdles for sensors due to their complex and diverse nature. Given that PFAS have diverse compositions and structures, a single interaction type is insufficient for thorough detection. Sophisticated methods that incorporate several identification components are required to provide PFAS sensing that is precise and dependable. These components should be able to distinguish between the distinct qualities of different types of PFAS simultaneously. Overcoming the PFAS variety and chemistry complexities is crucial for sensor development, creating a robust and adaptive platform that can handle the peculiarities of diverse PFAS compounds. Given the complex chemical differences across the PFAS family, researchers are continuously investigating novel approaches to improve the selectivity and sensitivity of sensors.

The choice between specific and broad-spectrum PFAS detection sensors is a critical factor in addressing the complexities of PFAS contamination. Sensors tailored to individual PFAS compounds, such as PFOS and PFOA, offer high specificity but may fall short of capturing the full spectrum of PFAS diversity. Alternatively, sensors designed to detect PFCAs, PFSAs, or total PFAS provide a broader perspective, ensuring a comprehensive approach for their monitoring. Striking the right balance between specificity and broad applicability is paramount, considering the varying prevalence of PFAS in different environments. Achieving this balance enables effective monitoring that caters to the specific chemical makeup of PFAS contaminants, while accommodating the diverse monitoring needs dictated by their widespread occurrence in various settings.

A combination of environmental parameters, nanomaterial characteristics, and interactions at the solute-sensing interface creates significant challenges in creating PFAS nano-sensors. Ecological aspects such as temperature, moisture, and pH levels substantially influence the functioning of nano-sensors. Maintaining the stability of sensors in various environments necessitates novel approaches, such as strong coatings and encapsulating methods to protect nanomaterials from external impacts. Nanomaterial parameters, such as size, composition, and surface features, substantially influence the sensitivity and selectivity of sensors. Ensuring the best performance of nano-sensors necessitates a thorough understanding of these features to create materials that improve the PFAS detection accuracy. Furthermore, the complex interactions at the solute-sensing surface highlight the need for surface engineering techniques that increase selective and reliable PFAS binding. Given the dynamic nature of environmental matrices, flexible sensor designs capable of handling various situations are required. Addressing these issues will be imperative in improving the reliability and effectiveness of PFAS nano-sensors, opening the path for their successful deployment in environmental monitoring applications.

The vital need for real-time evaluation during soil and wastewater remediation operations is driving the demand for field-deployable continuous monitoring sensors in the context of PFAS detection. Continuous monitoring is required by regulatory requirements to guarantee compliance with permissible PFAS concentrations. This pressing requirement has fueled research into creating robust sensors capable of withstanding various environmental conditions. These sensors are critical in measuring PFAS levels in real time, allowing operators to respond quickly to swings and departures from regulatory norms. The real-time data from these sensors enables proactive decision-making in environmental management, allowing effective and timely actions to mitigate PFAS pollution. The development of sensors is consistent with the overall objective of protecting environmental quality and human health in the face of PFAS issues.

Technological developments in semiconductor and metallic nanoparticles provide bright prospects for the PFAS sensing industry. The introduction of electrical, optical, and catalytic capabilities is the main reason for the revolutionary effect of these materials. Because of their unique qualities such as increased sensitivity and selectivity metallic nanoparticles and semiconductors are excellent choices for enhancing PFAS detection techniques. These cutting-edge materials may be used in sensor designs to increase their application, especially in analytical instruments. Furthermore, optical features improve the detection accuracy and electronic qualities allow effective signal transduction. Their catalytic functionality is a further factor increasing the total sensitivity of PFAS sensors. With enhanced capabilities for precise and effective PFAS detection in diverse environmental conditions, this development in sensor technology represents a substantial advancement. It addresses critical demands in ecological monitoring and management. Overall, deploying PFAS nano-sensors in environmental monitoring requires overcoming obstacles, including sensitivity and selectivity problems. Using the potential of these nano-sensors provides a viable path for the accurate and timely detection of PFAS, greatly aiding in cleanup operations and expanding our knowledge of their effects on the ecosystem.

Data availability

No primary research results, software or code have been included and no new data were generated or analysed as part of this review.

Conflicts of interest

There is no conflict of interest among authors.

Acknowledgements

References

1 X. Lim, Could the World Go PFAS-Free? Proposal to Ban 'Forever Chemicals' Fuels Debate, *Nature*, 2023, **620**(7972), 24–27, DOI: **10.1038/d41586-023-02444-5**.

2 C. Sonne, M. S. Bank, B. M. Jenssen, T. M. Cieseielski, J. Rinklebe, S. S. Lam, M. Hansen, R. Bossi, K. Gustavson and R. Dietz, PFAS Pollution Threatens Ecosystems Worldwide, *Science*, 2023, **379**(6635), 887–888, DOI: **10.1126/science.adh0934**.

3 K. I. Kirkwood-Donelson, J. N. Dodds, A. Schnetzer, N. Hall and E. S. Baker, Uncovering Per- and Polyfluoroalkyl Substances (PFAS) with Nontargeted Ion Mobility Spectrometry–Mass Spectrometry Analyses, *Sci. Adv.*, 2023, **9**(43), eadj7048, DOI: **10.1126/sciadv.adj7048**.

4 J. Oh, H.-M. Shin, K. Kannan, A. M. Calafat, R. J. Schmidt, I. Hertz-Picciotto and D. H. Bennett, Per- and Polyfluoroalkyl Substances (PFAS) in Serum of 2 to 5 Year-Old Children: Temporal Trends, Determinants, and Correlations with Maternal PFAS Concentrations, *Environ. Sci. Technol.*, 2024, **58**(7), 3151–3162, DOI: **10.1021/acs.est.3c08928**.

5 M. Sadia, I. Nollen, R. Helmus, T. L. ter Laak, F. Béen, A. Praetorius and A. P. van Wezel, Occurrence, Fate, and Related Health Risks of PFAS in Raw and Produced Drinking Water, *Environ. Sci. Technol.*, 2023, **57**(8), 3062–3074, DOI: **10.1021/acs.est.2c06015**.

6 J. Huang, Y. Shi, J. Xu, J. Zheng, F. Zhu, X. Liu and G. Ouyang, Hollow Covalent Organic Framework with "Shell-Confined" Environment for the Effective Removal of Anionic Per- and Polyfluoroalkyl Substances, *Adv. Funct. Mater.*, 2022, **32**(39), 2203171, DOI: **10.1002/adfm.202203171**.

7 Y. Shi, H. Mu, J. You, C. Han, H. Cheng, J. Wang, H. Hu and H. Ren, Confined Water–Encapsulated Activated Carbon for Capturing Short-Chain Perfluoroalkyl and Polyfluoroalkyl Substances from Drinking Water, *Proc. Natl. Acad. Sci. U. S. A.*, 2023, **120**(27), e2219179120, DOI: **10.1073/pnas.2219179120**.

8 S. F. Nakayama, M. Yoshikane, Y. Onoda, Y. Nishihama, M. Iwai-Shimada, M. Takagi, Y. Kobayashi and T. Isobe, Worldwide Trends in Tracing Poly- and Perfluoroalkyl Substances (PFAS) in the Environment, *TrAC, Trends Anal. Chem.*, 2019, **121**, 115410, DOI: **10.1016/j.trac.2019.02.011**.

9 B. Améduri and H. Hori, Recycling and the End of Life Assessment of Fluoropolymers: Recent Developments, Challenges and Future Trends, *Chem. Soc. Rev.*, 2023, **52**(13), 4208–4247, DOI: **10.1039/d2cs00763k**.

10 Y. He, J. Zhou, Y. Li, Y.-D. Yang, J. L. Sessler and X. Chi, Fluorinated Nonporous Adaptive Cages for the Efficient Removal of Perfluorooctanoic Acid from Aqueous Source Phases, *J. Am. Chem. Soc.*, 2024, **146**(9), 6225–6230, DOI: **10.1021/jacs.3c14213**.

11 C. Zhang, K. Yan, C. Fu, H. Peng, C. J. Hawker and A. K. Whittaker, Biological Utility of Fluorinated Compounds: From Materials Design to Molecular Imaging, Therapeutics and Environmental Remediation, *Chem. Rev.*, 2022, **122**(1), 167–208, DOI: **10.1021/acs.chemrev.1c00632**.

12 J. Han, L. Kiss, H. Mei, A. M. Remete, M. Ponikvar-Svet, D. M. Sedgwick, R. Roman, S. Fustero, H. Moriwaki and V. A. Soloshonok, Chemical Aspects of Human and Environmental Overload with Fluorine, *Chem. Rev.*, 2021, **121**(8), 4678–4742, DOI: **10.1021/acs.chemrev.0c01263**.

13 Y. Wen, Á. Rentería-Gómez, G. S. Day, M. F. Smith, T.-H. Yan, R. O. K. Ozdemir, O. Gutierrez, V. K. Sharma, X. Ma and H.-C. Zhou, Integrated Photocatalytic Reduction and Oxidation of Perfluorooctanoic Acid by Metal–Organic Frameworks: Key Insights into the Degradation Mechanisms, *J. Am. Chem. Soc.*, 2022, **144**(26), 11840–11850, DOI: **10.1021/jacs.2c04341**.

14 Z. Chen, Y.-L. Lu, L. Wang, J. Xu, J. Zhang, X. Xu, P. Cheng, S. Yang and W. Shi, Efficient Recognition and Removal of Persistent Organic Pollutants by a Bifunctional Molecular Material, *J. Am. Chem. Soc.*, 2023, **145**(1), 260–267, DOI: **10.1021/jacs.2c09866**.

15 O. Adu, X. Ma and V. K. Sharma, Bioavailability, Phytotoxicity and Plant Uptake of per-and Polyfluoroalkyl Substances (PFAS): A Review, *J. Hazard. Mater.*, 2023, **447**, 130805, DOI: **10.1016/j.jhazmat.2023.130805**.

16 Z.-M. Li, A. Roos, T. L. Serfass, C. Lee and K. Kannan, Concentrations of 45 Per- and Polyfluoroalkyl Substances in North American River Otters (*Lontra canadensis*) from West Virginia, USA, *Environ. Sci. Technol.*, 2024, **58**(4), 2089–2101, DOI: **10.1021/acs.est.3c09467**.

17 X. C. Hu, B. Ge, B. J. Ruyle, J. Sun and E. M. Sunderland, A Statistical Approach for Identifying Private Wells Susceptible to Perfluoroalkyl Substances (PFAS) Contamination, *Environ. Sci. Technol. Lett.*, 2021, **8**(7), 596–602, DOI: **10.1021/acs.estlett.1c00264**.

18 S. Y. Wee and A. Z. Aris, Revisiting the "Forever Chemicals", PFOA and PFOS Exposure in Drinking Water, *npj Clean Water*, 2023, **6**(1), 1–16, DOI: **10.1038/s41545-023-00274-6**.

19 X. C. Hu, A. K. Tokranov, J. Liddie, X. Zhang, P. Grandjean, J. E. Hart, F. Laden, Q. Sun, L. W. Y. Yeung and E. M. Sunderland, Tap Water Contributions to Plasma Concentrations of Poly- and Perfluoroalkyl Substances (PFAS) in a Nationwide Prospective Cohort of U.S. Women, *Environ. Health Perspect.*, 2019, **127**(6), 067006, DOI: **10.1289/EHP4093**.

20 E. A. Emmett, F. S. Shofer, H. Zhang, D. Freeman, C. Desai and L. M. Shaw, Community Exposure to Perfluorooctanoate: Relationships Between Serum

Concentrations and Exposure Sources, *J. Occup. Environ. Med.*, 2006, **48**(8), 759, DOI: **10.1097/01.jom.0000232486.07658.74**.

21 E. M. Bell, S. De Guise, J. R. McCutcheon, Y. Lei, M. Levin, B. Li, J. F. Rusling, D. A. Lawrence, J. M. Cavallari, C. O'Connell, B. Javidi, X. Wang and H. Ryu, Exposure, Health Effects, Sensing, and Remediation of the Emerging PFAS Contaminants – Scientific Challenges and Potential Research Directions, *Sci. Total Environ.*, 2021, **780**, 146399, DOI: **10.1016/j.scitotenv.2021.146399**.

22 B. Rudzanová, V. Thon, H. Vespalcová, C. J. Martyniuk, P. Piler, M. Zvonař, J. Klánová, L. Bláha and O. Adamovsky, Altered Transcriptome Response in PBMCs of Czech Adults Linked to Multiple PFAS Exposure: B Cell Development as a Target of PFAS Immunotoxicity, *Environ. Sci. Technol.*, 2024, **58**(1), 90–98, DOI: **10.1021/acs.est.3c05109**.

23 X. Tan, P. Dewapriya, P. Prasad, Y. Chang, X. Huang, Y. Wang, X. Gong, T. E. Hopkins, C. Fu, K. V. Thomas, H. Peng, A. K. Whittaker and C. Zhang, Efficient Removal of Perfluorinated Chemicals from Contaminated Water Sources Using Magnetic Fluorinated Polymer Sorbents, *Angew. Chem., Int. Ed.*, 2022, **61**(49), e202213071, DOI: **10.1002/anie.202213071**.

24 W. Xu, G. Li, H. Qu, C. Ma, H. Zhang, J. Cheng and H. Li, The Specific Removal of Perfluorooctanoic Acid Based on Pillar[5]Arene-Polymer-Packed Nanochannel Membrane, *ACS Nano*, 2023, **17**(19), 19305–19312, DOI: **10.1021/acsnano.3c06448**.

25 K. R. Taibl, A. L. Dunlop, D. B. Barr, Y.-Y. Li, S. M. Eick, K. Kannan, P. B. Ryan, M. Schroder, B. Rushing, T. Fennell, C.-J. Chang, Y. Tan, C. J. Marsit, D. P. Jones and D. Liang, Newborn Metabolomic Signatures of Maternal Per- and Polyfluoroalkyl Substance Exposure and Reduced Length of Gestation, *Nat. Commun.*, 2023, **14**(1), 3120, DOI: **10.1038/s41467-023-38710-3**.

26 Md. Al Amin, Z. Sobhani, Y. Liu, R. Dharmaraja, S. Chadalavada, R. Naidu, J. M. Chalker and C. Fang, Recent Advances in the Analysis of Per- and Polyfluoroalkyl Substances (PFAS)—A Review, *Environ. Technol. Innovation*, 2020, **19**, 100879, DOI: **10.1016/j.eti.2020.100879**.

27 M. Ateia, H. Wei and S. Andreescu, Sensors for Emerging Water Contaminants: Overcoming Roadblocks to Innovation, *Environ. Sci. Technol.*, 2024, **58**(6), 2636–2651, DOI: **10.1021/acs.est.3c09889**.

28 M. P. Ajith and P. Rajamani, Nanotechnology for Water Purification – Current Trends and Challenges, *J. Nanosci. Nanotechnol.*, 2021, **2**(2), 88–91, DOI: **10.33696/Nanotechnol.2.025**.

29 P. J. J. Alvarez, C. K. Chan, M. Elimelech, N. J. Halas and D. Villagrán, Emerging Opportunities for Nanotechnology to Enhance Water Security, *Nat. Nanotechnol.*, 2018, **13**(8), 634–641, DOI: **10.1038/s41565-018-0203-2**.

30 C. Villette, L. Maurer, J. Zumsteg, J. Mutterer, A. Wanko and D. Heintz, Mass Spectrometry Imaging for Biosolids Characterization to Assess Ecological or Health Risks before Reuse, *Nat. Commun.*, 2023, **14**(1), 4244, DOI: **10.1038/s41467-023-40051-0**.

31 Z. Wang, A. M. Buser, I. T. Cousins, S. Demattio, W. Drost, O. Johansson, K. Ohno, G. Patlewicz, A. M. Richard, G. W. Walker, G. S. White and E. Leinala, A New OECD Definition for Per- and Polyfluoroalkyl Substances, *Environ. Sci. Technol.*, 2021, **55**(23), 15575–15578, DOI: **10.1021/acs.est.1c06896**.

32 Y. Wang, S. B. Darling and J. Chen, Selectivity of Per- and Polyfluoroalkyl Substance Sensors and Sorbents in Water, *ACS Appl. Mater. Interfaces*, 2021, **13**(51), 60789–60814, DOI: **10.1021/acsami.1c16517**.

33 P. Mukherjee, K. Sathiyan, T. Zidki, M. N. Nadagouda and V. K. Sharma, Can Ultraviolet-Assisted Advanced Reduction Processes Effectively Destroy per- and Polyfluoroalkyl Substances in Real Water Matrices?, *Curr. Opin. Chem. Eng.*, 2023, **42**, 100971, DOI: **10.1016/j.coche.2023.100971**.

34 D. O'Hagan, Understanding Organofluorine Chemistry. An Introduction to the C–F Bond, *Chem. Soc. Rev.*, 2008, **37**(2), 308–319, DOI: **10.1039/B711844A**.

35 S. Joudan and R. J. Lundgren, Taking the "F" out of Forever Chemicals, *Science*, 2022, **377**(6608), 816–817, DOI: **10.1126/science.add1813**.

36 M. J. Bentel, Y. Yu, L. Xu, Z. Li, B. M. Wong, Y. Men and J. Liu, Defluorination of Per- and Polyfluoroalkyl Substances (PFASs) with Hydrated Electrons: Structural Dependence and Implications to PFAS Remediation and Management, *Environ. Sci. Technol.*, 2019, **53**(7), 3718–3728, DOI: **10.1021/acs.est.8b06648**.

37 M. Scheringer, Innovate beyond PFAS, *Science*, 2023, **381**(6655), 251, DOI: **10.1126/science.adj7475**.

38 W. A. Bernett, Hybridization Effects in Fluorocarbons, *J. Org. Chem.*, 1969, **34**(6), 1772–1776, DOI: **10.1021/jo01258a054**.

39 D. O'Hagan, Y. Wang, M. Skibinski and A. M. Z. Slawin, Influence of the difluoromethylene group (CF2) on the conformation and properties of selected organic compounds, *Pure Appl. Chem.*, 2012, **84**(7), 1587–1595, DOI: **10.1351/PAC-CON-11-09-26**.

40 Z. Du, S. Deng, Y. Bei, Q. Huang, B. Wang, J. Huang and G. Yu, Adsorption Behavior and Mechanism of Perfluorinated Compounds on Various Adsorbents—A Review, *J. Hazard. Mater.*, 2014, **274**, 443–454, DOI: **10.1016/j.jhazmat.2014.04.038**.

41 K. A. Barzen-Hanson, S. C. Roberts, S. Choyke, K. Oetjen, A. McAlees, N. Riddell, R. McCrindle, P. L. Ferguson, C. P. Higgins and J. A. Field, Discovery of 40 Classes of Per- and Polyfluoroalkyl Substances in Historical Aqueous Film-Forming Foams (AFFFs) and AFFF-Impacted Groundwater, *Environ. Sci. Technol.*, 2017, **51**(4), 2047–2057, DOI: **10.1021/acs.est.6b05843**.

42 J. Glüge, M. Scheringer, I. T. Cousins, J. C. DeWitt, G. Goldenman, D. Herzke, R. Lohmann, C. A. Ng, X. Trier and Z. Wang, An Overview of the Uses of Per- and Polyfluoroalkyl Substances (PFAS), *Environ. Sci.: Processes*

This journal is © The Royal Society of Chemistry 2025

J. Mater. Chem. A, 2025, **13**, 8246–8281 | **8275**

Impacts, 2020, **22**(12), 2345–2373, DOI: **10.1039/ D0EM00291G**.

43 S. C. E. Leung, D. Wanninayake, D. Chen, N.-T. Nguyen and Q. Li, Physicochemical Properties and Interactions of Perfluoroalkyl Substances (PFAS) – Challenges and Opportunities in Sensing and Remediation, *Sci. Total Environ.*, 2023, **905**, 166764, DOI: **10.1016/ j.scitotenv.2023.166764**.

44 L. Qi, R. Li, Y. Wu, X. Lin and G. Chen, Effect of Solution Chemistry on the Transport of Short-Chain and Long-Chain Perfluoroalkyl Carboxylic Acids (PFCAs) in Saturated Porous Media, *Chemosphere*, 2022, **303**, 135160, DOI: **10.1016/j.chemosphere.2022.135160**.

45 M. Ateia, A. Maroli, N. Tharayil and T. Karanfil, The Overlooked Short- and Ultrashort-Chain Poly- and Perfluorinated Substances: A Review, *Chemosphere*, 2019, **220**, 866–882, DOI: **10.1016/j.chemosphere.2018.12.186**.

46 K. Singh, N. Kumar, A. Kumar Yadav, R. Singh and K. Kumar, Per-and Polyfluoroalkyl Substances (PFAS) as a Health Hazard: Current State of Knowledge and Strategies in Environmental Settings across Asia and Future Perspectives, *Chem. Eng. J.*, 2023, **475**, 145064, DOI: **10.1016/j.cej.2023.145064**.

47 H. A. Kaboré, S. Vo Duy, G. Munoz, L. Méité, M. Desrosiers, J. Liu, T. K. Sory and S. Sauvé, Worldwide Drinking Water Occurrence and Levels of Newly-Identified Perfluoroalkyl and Polyfluoroalkyl Substances, *Sci. Total Environ.*, 2018, **616–617**, 1089–1100, DOI: **10.1016/j.scitotenv.2017.10.210**.

48 M. Sun, E. Arevalo, M. Strynar, A. Lindstrom, M. Richardson, B. Kearns, A. Pickett, C. Smith and D. R. U. Knappe, Legacy and Emerging Perfluoroalkyl Substances Are Important Drinking Water Contaminants in the Cape Fear River Watershed of North Carolina, *Environ. Sci. Technol. Lett.*, 2016, **3**(12), 415–419, DOI: **10.1021/acs.estlett.6b00398**.

49 C. Gremmel, T. Frömel and T. P. Knepper, HPLC-MS/MS Methods for the Determination of 52 Perfluoroalkyl and Polyfluoroalkyl Substances in Aqueous Samples, *Anal. Bioanal. Chem.*, 2017, **409**(6), 1643–1655, DOI: **10.1007/ s00216-016-0110-z**.

50 L. Rosenblum and S. C. Wendelken, *Method 533: Determination of Per- and Polyfluoroalkyl Substances in Drinking Water by Isotope Dilution Anion Exchange Solid Phase Extraction and Liquid Chromatography/Tandem Mass Spectrometry*, U.S. Environmental Protection Agency, Office of Ground Water and Drinking Water, Cincinnati, OH, 2019.

51 J. A. Shoemaker; P. E. Grimmett and B. K. Boutin, *Method 537: Determination of Selected Per- and Polyfluorinated Alkyl Substances in Drinking Water by Solid Phase Extraction and Liquid Chromatography/Tandem Mass Spectrometry (LC/MS/ MS)*, U.S. Environmental Protection Agency, Office of Research and Development, National Exposure Research Laboratory, Washington, D.C, 2018.

52 J. A. Shoemaker and D. R. Tettenhorst, *Method 537.1: Determination of Selected Per- and Polyfluorinated Alkyl Substances in Drinking Water by Solid Phase Extraction and Liquid Chromatography/Tandem Mass Spectrometry (LC/MS/ MS)*, U.S. Environmental Protection Agency, Office of Research and Development, National Exposure Research Laboratory, Washington, D.C, 2020.

53 M. Surma, W. Wiczkowski, E. Cieślik and H. Zieliński, Method Development for the Determination of PFOA and PFOS in Honey Based on the Dispersive Solid Phase Extraction (d-SPE) with Micro-UHPLC-MS/MS System, *Microchem. J.*, 2015, **121**, 150–156, DOI: **10.1016/ j.microc.2015.02.008**.

54 K. Bielicka-Daszkiewicz, Extraction Techniques Based on Solid State and Connected with Liquid Chromatography, *J. Liq. Chromatogr. Relat. Technol.*, 2016, **39**(10), 477–487, DOI: **10.1080/10826076.2016.1163501**.

55 R. Alzaga and J. M. Bayona, Determination of Perfluorocarboxylic Acids in Aqueous Matrices by Ion-Pair Solid-Phase Microextraction-in-Port Derivatization-Gas Chromatography-Negative Ion Chemical Ionization Mass Spectrometry, *J. Chromatogr. A*, 2004, **1042**(1), 155–162, DOI: **10.1016/j.chroma.2004.05.015**.

56 S. J. Smith, M. Lauria, C. P. Higgins, K. D. Pennell, J. Blotevogel and H. P. H. Arp, The Need to Include a Fluorine Mass Balance in the Development of Effective Technologies for PFAS Destruction, *Environ. Sci. Technol.*, 2024, **58**(6), 2587–2590, DOI: **10.1021/acs.est.3c10617**.

57 J. M. Flaherty, P. D. Connolly, E. R. Decker, S. M. Kennedy, M. E. Ellefson, W. K. Reagen and B. Szostek, Quantitative Determination of Perfluorooctanoic Acid in Serum and Plasma by Liquid Chromatography Tandem Mass Spectrometry, *J. Chromatogr. B*, 2005, **819**(2), 329–338, DOI: **10.1016/j.jchromb.2005.03.002**.

58 R. F. Menger, E. Funk, C. S. Henry and T. Borch, Sensors for Detecting Per- and Polyfluoroalkyl Substances (PFAS): A Critical Review of Development Challenges, Current Sensors, and Commercialization Obstacles, *Chem. Eng. J.*, 2021, **417**, 129133, DOI: **10.1016/j.cej.2021.129133**.

59 B. L. Li, J. Wang, H. L. Zou, S. Garaj, C. T. Lim, J. Xie, N. B. Li and D. T. Leong, Low-Dimensional Transition Metal Dichalcogenide Nanostructures Based Sensors, *Adv. Funct. Mater.*, 2016, **26**(39), 7034–7056, DOI: **10.1002/ adfm.201602136**.

60 P. J. Vikesland, Nanosensors for Water Quality Monitoring, *Nat. Nanotechnol.*, 2018, **13**(8), 651–660, DOI: **10.1038/ s41565-018-0209-9**.

61 E. Priyadarshini, A. M. Parambil, P. Rajamani, V. K. Ponnusamy and Y.-H. Chen, Exposure, Toxicological Mechanism of Endocrine Disrupting Compounds and Future Direction of Identification Using Nano-Architectonics, *Environ. Res.*, 2023, **225**, 115577, DOI: **10.1016/j.envres.2023.115577**.

62 2D Materials, a Matter for Chemists, *Nat. Nanotechnol.*, 2023, **18**(6), 535, DOI: **10.1038/s41565-023-01433-z**.

63 E. Schoolaert, R. Hoogenboom and K. De Clerck, Colorimetric Nanofibers as Optical Sensors, *Adv. Funct. Mater.*, 2017, **27**(38), 1702646, DOI: **10.1002/ adfm.201702646**.

8276 | *J. Mater. Chem. A*, 2025, **13**, 8246–8281

This journal is © The Royal Society of Chemistry 2025

64 C. Fang, R. Dharmarajan, M. Megharaj and R. Naidu, Gold Nanoparticle-Based Optical Sensors for Selected Anionic Contaminants, *TrAC, Trends Anal. Chem.*, 2017, **86**, 143–154, DOI: **10.1016/j.trac.2016.10.008**.

65 J. Liu, J. Du, Y. Su and H. Zhao, A Facile Solvothermal Synthesis of 3D Magnetic MoS2/Fe3O4 Nanocomposites with Enhanced Peroxidase-Mimicking Activity and Colorimetric Detection of Perfluorooctane Sulfonate, *Microchem. J.*, 2019, **149**, 104019, DOI: **10.1016/j.microc.2019.104019**.

66 H. Niu, S. Wang, Z. Zhou, Y. Ma, X. Ma and Y. Cai, Sensitive Colorimetric Visualization of Perfluorinated Compounds Using Poly(Ethylene Glycol) and Perfluorinated Thiols Modified Gold Nanoparticles, *Anal. Chem.*, 2014, **86**(9), 4170–4177, DOI: **10.1021/ac403406d**.

67 T. Liu, W. Wang, D. Jian, J. Li, H. Ding, D. Yi, F. Liu and S. Wang, Quantitative Remote and On-Site Hg^{2+} Detection Using the Handheld Smartphone Based Optical Fiber Fluorescence Sensor (SOFFS), *Sens. Actuators, B*, 2019, **301**, 127168, DOI: **10.1016/j.snb.2019.127168**.

68 M. Takayose, K. Akamatsu, H. Nawafune, T. Murashima and J. Matsui, Colorimetric Detection of Perfluorooctanoic Acid (PFOA) Utilizing Polystyrene-Modified Gold Nanoparticles, *Anal. Lett.*, 2012, **45**(18), 2856–2864, DOI: **10.1080/00032719.2012.696225**.

69 Q. Chen, P. Zhu, J. Xiong, L. Gao and K. Tan, A Sensitive and Selective Triple-Channel Optical Assay Based on Red-Emissive Carbon Dots for the Determination of PFOS, *Microchem. J.*, 2019, **145**, 388–396, DOI: **10.1016/j.microc.2018.11.003**.

70 Y. Li, Y. Lu, X. Zhang, H. Cao and Y. Huang, Cobalt-Embedded Nitrogen-Doped Carbon Nanosheets with Enhanced Oxidase-like Activity for Detecting Perfluorooctane Sulfonate, *Microchem. J.*, 2022, **181**, 107814, DOI: **10.1016/j.microc.2022.107814**.

71 E. E. Harrison and M. L. Waters, Detection and Differentiation of Per- and Polyfluoroalkyl Substances (PFAS) in Water Using a Fluorescent Imprint-and-Report Sensor Array, *Chem. Sci.*, 2023, **14**(4), 928–936, DOI: **10.1039/D2SC05685B**.

72 H. Feng, N. Wang, T. Tran.T, L. Yuan, J. Li and Q. Cai, Surface Molecular Imprinting on Dye–(NH2)–SiO2 NPs for Specific Recognition and Direct Fluorescent Quantification of Perfluorooctane Sulfonate, *Sens. Actuators, B*, 2014, **195**, 266–273, DOI: **10.1016/j.snb.2014.01.036**.

73 L. S. Walekar, M. Zheng, L. Zheng and M. Long, Selenium and Nitrogen Co-Doped Carbon Quantum Dots as a Fluorescent Probe for Perfluorooctanoic Acid, *Microchim. Acta*, 2019, **186**(5), 278, DOI: **10.1007/s00604-019-3400-2**.

74 A. Manayil Parambil, M. Nabeel Mattath, P. Rajamani, P. V. Pham, G. Kumar and V. K. Ponnusamy, Biogenic Fluorescent Carbon Dots Modulated Fabrication of Concatenate Logic Library and Pattern-Mediated Molecular Keypad Lock for Chemical Sensing Application, *Chem. Eng. J.*, 2023, **463**, 142354, DOI: **10.1016/j.cej.2023.142354**.

75 Z. Cheng, H. Dong, J. Liang, F. Zhang, X. Chen, L. Du and K. Tan, Highly Selective Fluorescent Visual Detection of Perfluorooctane Sulfonate *via* Blue Fluorescent Carbon Dots and Berberine Chloride Hydrate, *Spectrochim. Acta, Part A*, 2019, **207**, 262–269, DOI: **10.1016/j.saa.2018.09.028**.

76 Z. Zheng, H. Yu, W.-C. Geng, X.-Y. Hu, Y.-Y. Wang, Z. Li, Y. Wang and D.-S. Guo, Guanidinocalix[5]Arene for Sensitive Fluorescence Detection and Magnetic Removal of Perfluorinated Pollutants, *Nat. Commun.*, 2019, **10**(1), 5762, DOI: **10.1038/s41467-019-13775-1**.

77 Q. Chen, P. Zhu, J. Xiong, L. Gao and K. Tan, A New Dual-Recognition Strategy for Hybrid Ratiometric and Ratiometric Sensing Perfluorooctane Sulfonic Acid Based on High Fluorescent Carbon Dots with Ethidium Bromide, *Spectrochim. Acta, Part A*, 2020, **224**, 117362, DOI: **10.1016/j.saa.2019.117362**.

78 Z. Jiao, J. Li, L. Mo, J. Liang and H. Fan, A Molecularly Imprinted Chitosan Doped with Carbon Quantum Dots for Fluorometric Determination of Perfluorooctane Sulfonate, *Microchim. Acta*, 2018, **185**(10), 473, DOI: **10.1007/s00604-018-2996-y**.

79 Y. Hong, X. Chen, Y. Zhang, Y. Zhu, J. Sun, M. T. Swihart, K. Tan and L. Dong, One-Pot Hydrothermal Synthesis of High Quantum Yield Orange-Emitting Carbon Quantum Dots for Sensitive Detection of Perfluorinated Compounds, *New J. Chem.*, 2022, **46**(41), 19658–19666, DOI: **10.1039/D2NJ02907C**.

80 M. Yin, L. Che, S. Jiang, Q. Deng and S. Wang, Sensing of Perfluorinated Compounds Using a Functionalized Tricolor Upconversion Nanoparticle Based Fluorescence Sensor Array, *Environ. Sci.: Nano*, 2020, **7**(10), 3036–3046, DOI: **10.1039/D0EN00554A**.

81 J. Li, C. Zhang, M. Yin, Z. Zhang, Y. Chen, Q. Deng and S. Wang, Surfactant-Sensitized Covalent Organic Frameworks-Functionalized Lanthanide-Doped Nanocrystals: An Ultrasensitive Sensing Platform for Perfluorooctane Sulfonate, *ACS Omega*, 2019, **4**(14), 15947–15955, DOI: **10.1021/acsomega.9b01996**.

82 Q. Liu, A. Huang, N. Wang, G. Zheng and L. Zhu, Rapid Fluorometric Determination of Perfluorooctanoic Acid by Its Quenching Effect on the Fluorescence of Quantum Dots, *J. Lumin.*, 2015, **161**, 374–381, DOI: **10.1016/j.jlumin.2015.01.045**.

83 C. Fang, M. Megharaj and R. Naidu, Surface-Enhanced Raman Scattering (SERS) Detection of Fluorosurfactants in Firefighting Foams, *RSC Adv.*, 2016, **6**(14), 11140–11145, DOI: **10.1039/c5ra26114g**.

84 J. Tittel, F. Knechtel and E. Ploetz, Conquering Metal–Organic Frameworks by Raman Scattering Techniques, *Adv. Funct. Mater.*, 2024, **34**(43), 2307518, DOI: **10.1002/adfm.202307518**.

85 H. Wei, S. M. H. Abtahi and P. J. Vikesland, Plasmonic Colorimetric and SERS Sensors for Environmental Analysis, *Environ. Sci.: Nano*, 2015, **2**(2), 120–135, DOI: **10.1039/c4en00211c**.

This journal is © The Royal Society of Chemistry 2025

J. Mater. Chem. A, 2025, **13**, 8246–8281 | **8277**

86 J. P. Nolan and D. S. Sebba, Chapter 20 – Surface-Enhanced Raman Scattering (SERS) Cytometry, in *Methods in Cell Biology*, ed. Darzynkiewicz, Z., Holden, E., Orfao, A., Telford, W. and Wlodkowic, D., *Recent Advances in Cytometry, Part A*, Academic Press, 2011, vol. 102, pp. 515–532, DOI: 10.1016/B978-0-12-374912-3.00020-1.

87 V. Montes-García, M. A. Squillaci, M. Diez-Castellnou, Q. K. Ong, F. Stellacci and P. Samorì, Chemical Sensing with Au and Ag Nanoparticles, *Chem. Soc. Rev.*, 2021, **50**(2), 1269–1304, DOI: 10.1039/d0cs01112f.

88 T. Lazarević-Pašti, T. Tasić, V. Milanković and N. Potkonjak, Molecularly Imprinted Plasmonic-Based Sensors for Environmental Contaminants—Current State and Future Perspectives, *Chemosensors*, 2023, **11**(1), 35, DOI: 10.3390/chemosensors11010035.

89 N. Cennamo, G. D'Agostino, G. Porto, A. Biasiolo, C. Perri, F. Arcadio and L. Zeni, A Molecularly Imprinted Polymer on a Plasmonic Plastic Optical Fiber to Detect Perfluorinated Compounds in Water, *Sensors*, 2018, **18**(6), 1836, DOI: 10.3390/s18061836.

90 R. B. Clark and J. E. Dick, Electrochemical Sensing of Perfluorooctanesulfonate (PFOS) Using Ambient Oxygen in River Water, *ACS Sens.*, 2020, **5**(11), 3591–3598, DOI: 10.1021/acssensors.0c01894.

91 R. B. Clark and J. E. Dick, Towards Deployable Electrochemical Sensors for Per- and Polyfluoroalkyl Substances (PFAS), *Chem. Commun.*, 2021, **57**(66), 8121–8130, DOI: 10.1039/D1CC02641K.

92 P. Mukherjee, K. Sathiyan, T. Zidki, M. N. Nadagouda and V. K. Sharma, Electrochemical Degradation of Per- and Poly-Fluoroalkyl Substances in the Presence of Natural Organic Matter, *Sep. Purif. Technol.*, 2023, **325**, 124639, DOI: 10.1016/j.seppur.2023.124639.

93 A. K. Yadav, D. Verma and P. R. Solanki, Enhanced Electrochemical Biosensing of the Sp17 Cancer Biomarker in Serum Samples *via* Engineered Two-Dimensional MoS2 Nanosheets on the Reduced Graphene Oxide Interface, *ACS Appl. Bio Mater.*, 2023, **6**(10), 4250–4268, DOI: 10.1021/acsabm.3c00464.

94 C. Zhu, G. Yang, H. Li, D. Du and Y. Lin, Electrochemical Sensors and Biosensors Based on Nanomaterials and Nanostructures, *Anal. Chem.*, 2015, **87**(1), 230–249, DOI: 10.1021/ac5039863.

95 M. A. A. Mamun and M. R. Yuce, Recent Progress in Nanomaterial Enabled Chemical Sensors for Wearable Environmental Monitoring Applications, *Adv. Funct. Mater.*, 2020, **30**(51), 2005703, DOI: 10.1002/adfm.202005703.

96 I.-H. Cho, D. H. Kim and S. Park, Electrochemical Biosensors: Perspective on Functional Nanomaterials for on-Site Analysis, *Biomater. Res.*, 2020, **24**(1), 6, DOI: 10.1186/s40824-019-0181-y.

97 R. Ranaweera, C. Ghafari and L. Luo, Bubble-Nucleation-Based Method for the Selective and Sensitive Electrochemical Detection of Surfactants, *Anal. Chem.*, 2019, **91**(12), 7744–7748, DOI: 10.1021/acs.analchem.9b01060.

98 Y. Gao, W. Gou, W. Zeng, W. Chen, J. Jiang and J. Lu, Determination of Perfluorooctanesulfonic Acid in Water by Polydopamine Molecularly Imprinted/Gold Nanoparticles Sensor, *Microchem. J.*, 2023, **187**, 108378, DOI: 10.1016/j.microc.2022.108378.

99 M. Pierpaoli, M. Szopińska, A. Olejnik, J. Ryl, S. Fudala-Ksiażek, A. Łuczkiewicz and R. Bogdanowicz, Engineering Boron and Nitrogen Codoped Carbon Nanoarchitectures to Tailor Molecularly Imprinted Polymers for PFOS Determination, *J. Hazard. Mater.*, 2023, **458**, 131873, DOI: 10.1016/j.jhazmat.2023.131873.

100 R. Kazemi, E. I. Potts and J. E. Dick, Quantifying Interferent Effects on Molecularly Imprinted Polymer Sensors for Per- and Polyfluoroalkyl Substances (PFAS), *Anal. Chem.*, 2020, **92**(15), 10597–10605, DOI: 10.1021/acs.analchem.0c01565.

101 J. Gong, T. Fang, D. Peng, A. Li and L. Zhang, A Highly Sensitive Photoelectrochemical Detection of Perfluorooctanic Acid with Molecularly Imprinted Polymer-Functionalized Nanoarchitectured Hybrid of AgI–BiOI Composite, *Biosens. Bioelectron.*, 2015, **73**, 256–263, DOI: 10.1016/j.bios.2015.06.008.

102 T. T. Tran, J. Li, H. Feng, J. Cai, L. Yuan, N. Wang and Q. Cai, Molecularly Imprinted Polymer Modified TiO$_2$ Nanotube Arrays for Photoelectrochemical Determination of Perfluorooctane Sulfonate (PFOS), *Sens. Actuators, B*, 2014, **190**, 745–751, DOI: 10.1016/j.snb.2013.09.048.

103 X. Li, X. Wang, T. Fang, L. Zhang and J. Gong, Disposable Photoelectrochemical Sensing Strip for Highly Sensitive Determination of Perfluorooctane Sulfonyl Fluoride on Functionalized Screen-Printed Carbon Electrode, *Talanta*, 2018, **181**, 147–153, DOI: 10.1016/j.talanta.2018.01.005.

104 Y. H. Cheng, D. Barpaga, J. A. Soltis, V. Shutthanandan, R. Kargupta, K. S. Han, B. P. McGrail, R. K. Motkuri, S. Basuray and S. Chatterjee, Metal–Organic Framework-Based Microfluidic Impedance Sensor Platform for Ultrasensitive Detection of Perfluorooctanesulfonate, *ACS Appl. Mater. Interfaces*, 2020, **12**(9), 10503–10514, DOI: 10.1021/acsami.9b22445.

105 S. Chen, A. Li, L. Zhang and J. Gong, Molecularly Imprinted Ultrathin Graphitic Carbon Nitride Nanosheets-Based Electrochemiluminescence Sensing Probe for Sensitive Detection of Perfluorooctanoic Acid, *Anal. Chim. Acta*, 2015, **896**, 68–77, DOI: 10.1016/j.aca.2015.09.022.

106 G. J. Islam and D. W. M. Arrigan, Voltammetric Selectivity in Detection of Ionized Perfluoroalkyl Substances at Micro-Interfaces between Immiscible Electrolyte Solutions, *ACS Sens.*, 2022, **7**(10), 2960–2967, DOI: 10.1021/acssensors.2c01100.

107 D. Lu, D. Z. Zhu, H. Gan, Z. Yao, J. Luo, S. Yu and P. Kurup, An Ultra-Sensitive Molecularly Imprinted Polymer (MIP) and Gold Nanostars (AuNS) Modified Voltammetric Sensor for Facile Detection of Perfluorooctance Sulfonate (PFOS) in Drinking Water, *Sens. Actuators, B*, 2022, **352**, 131055, DOI: 10.1016/j.snb.2021.131055.

108 N. Karimian, A. M. Stortini, L. M. Moretto, C. Costantino, S. Bogialli and P. Ugo, Electrochemosensor for Trace Analysis of Perfluorooctanesulfonate in Water Based on

8278 | *J. Mater. Chem. A*, 2025, **13**, 8246–8281

This journal is © The Royal Society of Chemistry 2025

a Molecularly Imprinted Poly(o-Phenylenediamine) Polymer, *ACS Sens.*, 2018, **3**(7), 1291–1298, DOI: **10.1021/acssensors.8b00154**.

109 C. Fang, Z. Chen, M. Megharaj and R. Naidu, Potentiometric Detection of AFFFs Based on MIP, *Environ. Technol. Innovation*, 2016, **5**, 52–59, DOI: **10.1016/j.eti.2015.12.003**.

110 M. W. Glasscott, K. J. Vannoy, R. Kazemi, M. D. Verber and J. E. Dick, μ-MIP: Molecularly Imprinted Polymer-Modified Microelectrodes for the Ultrasensitive Quantification of GenX (HFPO-DA) in River Water, *Environ. Sci. Technol. Lett.*, 2020, **7**(7), 489–495, DOI: **10.1021/acs.estlett.0c00341**.

111 Y. Wang, Y. Rong, T. Ma, L. Li, X. Li, P. Zhu, S. Zhou, J. Yu and Y. Zhang, Photoelectrochemical Sensors Based on Paper and Their Emerging Applications in Point-of-Care Testing, *Biosens. Bioelectron.*, 2023, **236**, 115400, DOI: **10.1016/j.bios.2023.115400**.

112 A. Qureshi, T. Shaikh and J. H. Niazi, Semiconductor Quantum Dots in Photoelectrochemical Sensors from Fabrication to Biosensing Applications, *Analyst*, 2023, **148**(8), 1633–1652, DOI: **10.1039/D2AN01690G**.

113 H.-Y. Wang, Y.-T. Xu, B. Wang, S.-Y. Yu, X.-M. Shi, W.-W. Zhao, D. Jiang, H.-Y. Chen and J.-J. Xu, A Photoelectrochemical Nanoreactor for Single-Cell Sampling and Near Zero-Background Faradaic Detection of Intracellular microRNA, *Angew. Chem.*, 2022, **134**(47), e202212752, DOI: **10.1002/ange.202212752**.

114 Y. Luo, Y. Hao, P. Zhang, Y. Zhang, R. Zeng, S. Chen and M. Xu, Chemiluminescence-Driven Photoelectrochemical Sensor: A Mini Review, *Electroanalysis*, 2024, **36**(1), e202300257, DOI: **10.1002/elan.202300257**.

115 Y. Zang, J. Lei and H. Ju, Principles and Applications of Photoelectrochemical Sensing Strategies Based on Biofunctionalized Nanostructures, *Biosens. Bioelectron.*, 2017, **96**, 8–16, DOI: **10.1016/j.bios.2017.04.030**.

116 G. Moro, D. Cristofori, F. Bottari, E. Cattaruzza, K. De Wael and L. M. Moretto, Redesigning an Electrochemical MIP Sensor for PFOS: Practicalities and Pitfalls, *Sensors*, 2019, **19**(20), 4433, DOI: **10.3390/s19204433**.

117 T.-Y. Chi, Z. Chen and J. Kameoka, Perfluorooctanesulfonic Acid Detection Using Molecularly Imprinted Polyaniline on a Paper Substrate, *Sensors*, 2020, **20**(24), 7301, DOI: **10.3390/s20247301**.

118 L. I. FitzGerald, J. F. Olorunyomi, R. Singh and C. M. Doherty, Towards Solving the PFAS Problem: The Potential Role of Metal–Organic Frameworks, *ChemSusChem*, 2022, **15**(19), e202201136, DOI: **10.1002/cssc.202201136**.

119 E. Karbassiyazdi, M. Kasula, S. Modak, J. Pala, M. Kalantari, A. Altaee, M. R. Esfahani and A. Razmjou, A Juxtaposed Review on Adsorptive Removal of PFAS by Metal-Organic Frameworks (MOFs) with Carbon-Based Materials, Ion Exchange Resins, and Polymer Adsorbents, *Chemosphere*, 2023, **311**, 136933, DOI: **10.1016/j.chemosphere.2022.136933**.

120 M. H. Hassan, R. Khan and S. Andreescu, Advances in Electrochemical Detection Methods for Measuring Contaminants of Emerging Concerns, *Electrochem. Sci. Adv.*, 2022, **2**(6), e2100184, DOI: **10.1002/elsa.202100184**.

121 S.-M. Yoo, Y.-M. Jeon and S.-Y. Heo, Electrochemiluminescence Systems for the Detection of Biomarkers: Strategical and Technological Advances, *Biosensors*, 2022, **12**(9), 738, DOI: **10.3390/bios12090738**.

122 M. Yadav, F. J. Osonga and O. A. Sadik, Unveiling Nano-Empowered Catalytic Mechanisms for PFAS Sensing, Removal and Destruction in Water, *Sci. Total Environ.*, 2024, **912**, 169279, DOI: **10.1016/j.scitotenv.2023.169279**.

123 A. M. Parambil, A. Prasad, A. K. Tomar, I. Ghosh and P. Rajamani, Biogenic Carbon Dots: A Novel Mechanistic Approach to Combat Multidrug-Resistant Critical Pathogens on the Global Priority List, *J. Mater. Chem. B*, 2024, **12**(1), 202–221, DOI: **10.1039/D3TB02374E**.

124 Y. Chen, Y. Cao, C. Ma and J.-J. Zhu, Carbon-Based Dots for Electrochemiluminescence Sensing, *Mater. Chem. Front.*, 2020, **4**(2), 369–385, DOI: **10.1039/C9QM00572B**.

125 J. S. Lee, S. G. Kim, J. Jun, D. H. Shin and J. Jang, Aptamer-Functionalized Multidimensional Conducting-Polymer Nanoparticles for an Ultrasensitive and Selective Field-Effect-Transistor Endocrine-Disruptor Sensors, *Adv. Funct. Mater.*, 2014, **24**(39), 6145–6153, DOI: **10.1002/adfm.201401166**.

126 S. Liang, A. B. Kinghorn, M. Voliotis, J. K. Prague, J. D. Veldhuis, K. Tsaneva-Atanasova, C. A. McArdle, R. H. W. Li, A. E. G. Cass, W. S. Dhillo and J. A. Tanner, Measuring Luteinising Hormone Pulsatility with a Robotic Aptamer-Enabled Electrochemical Reader, *Nat. Commun.*, 2019, **10**(1), 852, DOI: **10.1038/s41467-019-08799-6**.

127 J. Zhang and Y. Cao, Chapter 6 – Aptasensors, in *Nano-Inspired Biosensors for Protein Assay With Clinical Applications*, ed. Li, G., Elsevier, 2019, pp. 139–166, DOI: **10.1016/B978-0-12-815053-5.00006-4**.

128 C. Reinemann and B. Strehlitz, Aptamer-Modified Nanoparticles and Their Use in Cancer Diagnostics and Treatment, *Swiss Med. Wkly.*, 2013, **143**(0102), w13908, DOI: **10.4414/smw.2014.13908**.

129 J. Park, K.-A. Yang, Y. Choi and J. K. Choe, Novel ssDNA Aptamer-Based Fluorescence Sensor for Perfluorooctanoic Acid Detection in Water, *Environ. Int.*, 2022, **158**, 107000, DOI: **10.1016/j.envint.2021.107000**.

130 Z. R. Churcher and P. E. Johnson, *NMR for Non-Experts; A Practical Guide for Applying NMR Methods in Studies of Aptamer-Ligand Interactions*, 2020.

131 M. A. D. Neves, O. Reinstein and P. E. Johnson, Defining a Stem Length-Dependent Binding Mechanism for the Cocaine-Binding Aptamer. A Combined NMR and Calorimetry Study, *Biochemistry*, 2010, **49**(39), 8478–8487, DOI: **10.1021/bi100952k**.

132 N. Chaudhary, A. K. Yadav, D. Verma, J. Gopal Sharma, R. Solanki and P. An, Electrochemical Immunosensor Based on a Nanostructured Lanthanum Oxide-Substituted Reduced Graphene Oxide Interface for Ultralow Ciprofloxacin Detection in Milk Samples, *Mater. Adv.*, 2024, **5**(4), 1597–1613, DOI: **10.1039/D3MA00556A**.

This journal is © The Royal Society of Chemistry 2025

J. Mater. Chem. A, 2025, **13**, 8246–8281 | **8279**

133 B. J. Yakes, J. Buijs, C. T. Elliott and K. Campbell, Surface Plasmon Resonance Biosensing: Approaches for Screening and Characterising Antibodies for Food Diagnostics, *Talanta*, 2016, **156–157**, 55–63, DOI: **10.1016/j.talanta.2016.05.008**.

134 N. Cennamo, L. Zeni, P. Tortora, M. E. Regonesi, A. Giusti, M. Staiano, S. D'Auria and A. Varriale, A High Sensitivity Biosensor to Detect the Presence of Perfluorinated Compounds in Environment, *Talanta*, 2018, **178**, 955–961, DOI: **10.1016/j.talanta.2017.10.034**.

135 W. Xia, Y.-J. Wan, X. Wang, Y. Li, W.-J. Yang, C.-X. Wang and S. Xu, Sensitive Bioassay for Detection of PPARα Potentially Hazardous Ligands with Gold Nanoparticle Probe, *J. Hazard. Mater.*, 2011, **192**(3), 1148–1154, DOI: **10.1016/j.jhazmat.2011.06.023**.

136 T. Zhang, H. Zhao, A. Lei and X. Quan, Electrochemical Biosensor for Detection of Perfluorooctane Sulfonate Based on Inhibition Biocatalysis of Enzymatic Fuel Cell, *Electrochemistry*, 2014, **82**(2), 94–99, DOI: **10.5796/electrochemistry.82.94**.

137 J. L. Alesio, A. Slitt and G. D. Bothun, Critical New Insights into the Binding of Poly- and Perfluoroalkyl Substances (PFAS) to Albumin Protein, *Chemosphere*, 2022, **287**, 131979, DOI: **10.1016/j.chemosphere.2021.131979**.

138 J. Zhang, Y. Wan, Y. Li, Q. Zhang, S. Xu, H. Zhu and B. Shu, A Rapid and High-Throughput Quantum Dots Bioassay for Monitoring of Perfluorooctane Sulfonate in Environmental Water Samples, *Environ. Pollut.*, 2011, **159**(5), 1348–1353, DOI: **10.1016/j.envpol.2011.01.011**.

139 A. Román Santiago, S. Yin, J. Elbert, J. Lee, D. Shukla and X. Su, Imparting Selective Fluorophilic Interactions in Redox Copolymers for the Electrochemically Mediated Capture of Short-Chain Perfluoroalkyl Substances, *J. Am. Chem. Soc.*, 2023, **145**(17), 9508–9519, DOI: **10.1021/jacs.2c10963**.

140 E. Kumarasamy, I. M. Manning, L. B. Collins, O. Coronell and F. A. Leibfarth, Ionic Fluorogels for Remediation of Per- and Polyfluorinated Alkyl Substances from Water, *ACS Cent. Sci.*, 2020, **6**(4), 487–492, DOI: **10.1021/acscentsci.9b01224**.

141 T. S. Erkal, N. Shamsuddin, S. Kirmizialtin and A. O. Yazaydin, Computational Investigation of Structure–Function Relationship in Fluorine-Functionalized MOFs for PFOA Capture from Water, *J. Phys. Chem. C*, 2023, **127**(6), 3204–3216, DOI: **10.1021/acs.jpcc.2c07737**.

142 X. Lei, Q. Lian, X. Zhang, T. K. Karsili, W. Holmes, Y. Chen, M. E. Zappi and D. D. Gang, A Review of PFAS Adsorption from Aqueous Solutions: Current Approaches, Engineering Applications, Challenges, and Opportunities, *Environ. Pollut.*, 2023, **321**, 121138, DOI: **10.1016/j.envpol.2023.121138**.

143 M. G. Evich, M. J. B. Davis, J. P. McCord, B. Acrey, J. A. Awkerman, D. R. U. Knappe, A. B. Lindstrom, T. F. Speth, C. Tebes-Stevens, M. J. Strynar, Z. Wang, E. J. Weber, W. M. Henderson and J. W. Washington, Per- and Polyfluoroalkyl Substances in the Environment, *Science*, 2022, **375**(6580), eabg9065, DOI: **10.1126/science.abg9065**.

144 I. M. Manning, N. Guan Pin Chew, H. P. Macdonald, K. E. Miller, M. J. Strynar, O. Coronell and F. A. Leibfarth, Hydrolytically Stable Ionic Fluorogels for High-Performance Remediation of Per- and Polyfluoroalkyl Substances (PFAS) from Natural Water, *Angew. Chem., Int. Ed.*, 2022, **61**(41), e202208150, DOI: **10.1002/anie.202208150**.

145 Y. He, X. Cheng, S. J. Gunjal and C. Zhang, Advancing PFAS Sorbent Design: Mechanisms, Challenges, and Perspectives, *ACS Mater. Au*, 2023, **4**(2), 108–114, DOI: **10.1021/acsmaterialsau.3c00066**.

146 C. Moreno-Castilla, Adsorption of Organic Molecules from Aqueous Solutions on Carbon Materials, *Carbon*, 2004, **42**(1), 83–94, DOI: **10.1016/j.carbon.2003.09.022**.

147 D. D. Chronopoulos, A. Bakandritsos, M. Pykal, R. Zbořil and M. Otyepka, Chemistry, Properties, and Applications of Fluorographene, *Appl. Mater. Today*, 2017, **9**, 60–70, DOI: **10.1016/j.apmt.2017.05.004**.

148 S. Garde, Hydrophobic Interactions in Context, *Nature*, 2015, **517**(7534), 277–279, DOI: **10.1038/517277a**.

149 C. You, C. Jia and G. Pan, Effect of Salinity and Sediment Characteristics on the Sorption and Desorption of Perfluorooctane Sulfonate at Sediment-Water Interface, *Environ. Pollut.*, 2010, **158**(5), 1343–1347, DOI: **10.1016/j.envpol.2010.01.009**.

150 W. Wang, G. Rhodes, W. Zhang, X. Yu, B. J. Teppen and H. Li, Implication of Cation-Bridging Interaction Contribution to Sorption of Perfluoroalkyl Carboxylic Acids by Soils, *Chemosphere*, 2022, **290**, 133224, DOI: **10.1016/j.chemosphere.2021.133224**.

151 M. Kanduč, E. Schneck and C. Stubenrauch, Intersurfactant H-Bonds between Head Groups of *n*-Dodecyl-β-d-Maltoside at the Air-Water Interface, *J. Colloid Interface Sci.*, 2021, **586**, 588–595, DOI: **10.1016/j.jcis.2020.10.125**.

152 R. Patel, L. E. Saab, P. J. Brahana, K. T. Valsaraj and B. Bharti, Interfacial Activity and Surface pK_a of Perfluoroalkyl Carboxylic Acids (PFCAs), *Langmuir*, 2024, **40**(7), 3651–3658, DOI: **10.1021/acs.langmuir.3c03398**.

153 J. Hammer and S. Endo, Volatility and Nonspecific van Der Waals Interaction Properties of Per- and Polyfluoroalkyl Substances (PFAS): Evaluation Using Hexadecane/Air Partition Coefficients, *Environ. Sci. Technol.*, 2022, **56**(22), 15737–15745, DOI: **10.1021/acs.est.2c05804**.

154 D. Zhu, S. Hyun, J. J. Pignatello and L. S. Lee, Evidence for Pi-Pi Electron Donor–Acceptor Interactions between Pi-Donor Aromatic Compounds and Pi-Acceptor Sites in Soil Organic Matter through pH Effects on Sorption, *Environ. Sci. Technol.*, 2004, **38**(16), 4361–4368, DOI: **10.1021/es035379e**.

155 L. Zdražil, Z. Baďura, M. Langer, S. Kalytchuk, D. Panáček, M. Scheibe, Š. Kment, H. Kmentová, M. A. Thottappali, E. Mohammadi, M. Medveď, A. Bakandritsos, G. Zoppellaro, R. Zbořil and M. Otyepka, Magnetic Polaron States in Photoluminescent Carbon Dots Enable

8280 | *J. Mater. Chem. A*, 2025, **13**, 8246–8281

This journal is © The Royal Society of Chemistry 2025

Hydrogen Peroxide Photoproduction, *Small*, 2023, **19**(32), 2206587, DOI: **10.1002/smll.202206587**.

156 N. O. Weiss, H. Zhou, L. Liao, Y. Liu, S. Jiang, Y. Huang and X. Duan, Graphene: An Emerging Electronic Material, *Adv. Mater.*, 2012, **24**(43), 5782–5825, DOI: **10.1002/adma.201201482**.

157 L. Zdražil, D. Panáček, V. Šedajová, Z. Baďura, M. Langer, M. Medveď, M. Paloncýová, M. Scheibe, S. Kalytchuk, G. Zoppellaro, Š. Kment, A. Cadranel, A. Bakandritsos, D. M. Guldi, M. Otyepka and R. Zbořil, Carbon Dots Enabling Parts-Per-Billion Sensitive and Ultraselective Photoluminescence Lifetime-Based Sensing of Inorganic Mercury, *Adv. Opt. Mater.*, 2023, **11**(21), 2300750, DOI: **10.1002/adom.202300750**.

158 M. D. Hossain, Z. Liu, M. Zhuang, X. Yan, G.-L. Xu, C. A. Gadre, A. Tyagi, I. H. Abidi, C.-J. Sun, H. Wong, A. Guda, Y. Hao, X. Pan, K. Amine and Z. Luo, Rational Design of Graphene-Supported Single Atom Catalysts for Hydrogen Evolution Reaction, *Adv. Energy Mater.*, 2019, **9**(10), 1803689, DOI: **10.1002/aenm.201803689**.

159 A. K. Prabhakar, M. P. Ajith, A. Ananthanarayanan, P. Routh, B. C. Mohan and A. M. Thamizhchelvan, Ball-Milled Graphene Quantum Dots for Enhanced Anti-Cancer Drug Delivery, *OpenNano*, 2022, **8**, 100072, DOI: **10.1016/j.onano.2022.100072**.

160 M. Zhou, Y. Jiang, G. Wang, W. Wu, W. Chen, P. Yu, Y. Lin, J. Mao and L. Mao, Single-Atom Ni-N$_4$ Provides a Robust Cellular NO Sensor, *Nat. Commun.*, 2020, **11**(1), 3188, DOI: **10.1038/s41467-020-17018-6**.

161 A. M. Parambil, S. Rajan, P.-C. Huang, U. Shashikumar, P.-C. Tsai, P. Rajamani, Y.-C. Lin and V. K. Ponnusamy, Carbon and Graphene Quantum Dots Based Architectonics for Efficient Aqueous Decontamination by Adsorption Chromatography Technique – Current State and Prospects, *Environ. Res.*, 2024, **251**, 118541, DOI: **10.1016/j.envres.2024.118541**.

162 J. Lee, C. Kim, C. Liu, M. S. Wong, N. L. Cápiro, K. D. Pennell and J. D. Fortner, Ultra-High Capacity, Multifunctional Nanoscale Sorbents for PFOA and PFOS Treatment, *npj Clean Water*, 2023, **6**(1), 1–10, DOI: **10.1038/s41545-023-00263-9**.

163 M. Gar Alalm and D. C. Boffito, Mechanisms and Pathways of PFAS Degradation by Advanced Oxidation and Reduction Processes: A Critical Review, *Chem. Eng. J.*, 2022, **450**, 138352, DOI: **10.1016/j.cej.2022.138352**.

164 M. Chaudhary, M. Sela-Adler, A. Ronen and O. Nir, Efficient PFOA Removal from Drinking Water by a Dual-Functional Mixed-Matrix-Composite Nanofiltration Membrane, *npj Clean Water*, 2023, **6**(1), 1–10, DOI: **10.1038/s41545-023-00286-2**.

165 A. M. Parambil and P. Rajamani, Carbon Dots: A Promising Path towards Environmental Sustainability, *Environ. Sci.:Adv.*, 2024, **3**(11), 1513–1523, DOI: **10.1039/D4VA00273C**.

166 A. Berhanu, I. Mutanda, J. Taolin, M. A. Qaria, B. Yang and D. Zhu, A Review of Microbial Degradation of Per- and Polyfluoroalkyl Substances (PFAS): Biotransformation Routes and Enzymes, *Sci. Total Environ.*, 2023, **859**, 160010, DOI: **10.1016/j.scitotenv.2022.160010**.

167 K. Sivagami, P. Sharma, A. V. Karim, G. Mohanakrishna, S. Karthika, G. Divyapriya, R. Saravanathamizhan and A. N. Kumar, Electrochemical-Based Approaches for the Treatment of Forever Chemicals: Removal of Perfluoroalkyl and Polyfluoroalkyl Substances (PFAS) from Wastewater, *Sci. Total Environ.*, 2023, **861**, 160440, DOI: **10.1016/j.scitotenv.2022.160440**.

This journal is © The Royal Society of Chemistry 2025

J. Mater. Chem. A, 2025, **13**, 8246–8281 | **8281**